



HAL
open science

Constitutive HIF-1 α expression in the epidermis fuels proliferation and is essential for effective barrier formation

Julia Boix, Jana Knuever, Nadine Niehoff, Ayesha Sen, David Pla-Martin, Olivier R Baris, Julia Etich, Bent Brachvogel, Harshita Kaul, Dirk Isbrandt, et al.

► **To cite this version:**

Julia Boix, Jana Knuever, Nadine Niehoff, Ayesha Sen, David Pla-Martin, et al.. Constitutive HIF-1 α expression in the epidermis fuels proliferation and is essential for effective barrier formation. Journal of Investigative Dermatology, 2024, Online ahead of print. 10.1016/j.jid.2024.09.022 . hal-04833011

HAL Id: hal-04833011

<https://hal.science/hal-04833011v1>

Submitted on 12 Dec 2024

HAL is a multi-disciplinary open access archive for the deposit and dissemination of scientific research documents, whether they are published or not. The documents may come from teaching and research institutions in France or abroad, or from public or private research centers.

L'archive ouverte pluridisciplinaire **HAL**, est destinée au dépôt et à la diffusion de documents scientifiques de niveau recherche, publiés ou non, émanant des établissements d'enseignement et de recherche français ou étrangers, des laboratoires publics ou privés.

Journal Pre-proof

Constitutive HIF-1 α expression in the epidermis fuels proliferation and is essential for effective barrier formation

Julia Boix, Jana Knuever, Nadine Niehoff, Ayesha Sen, David Pla-Martin, Olivier R. Baris, Julia Etich, Bent Brachvogel, Harshita Kaul, Dirk Isbrandt, Ekaterina Soroka, Hisham Bazzi, Roland H. Wenger, Patrick Giavalisco, Rudolf J. Wiesner

PII: S0022-202X(24)02951-8

DOI: <https://doi.org/10.1016/j.jid.2024.09.022>

Reference: JID 4540

To appear in: *The Journal of Investigative Dermatology*

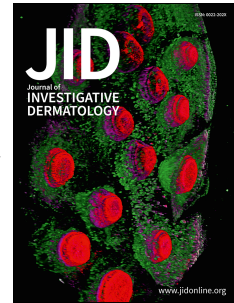
Received Date: 29 June 2023

Revised Date: 15 September 2024

Accepted Date: 30 September 2024

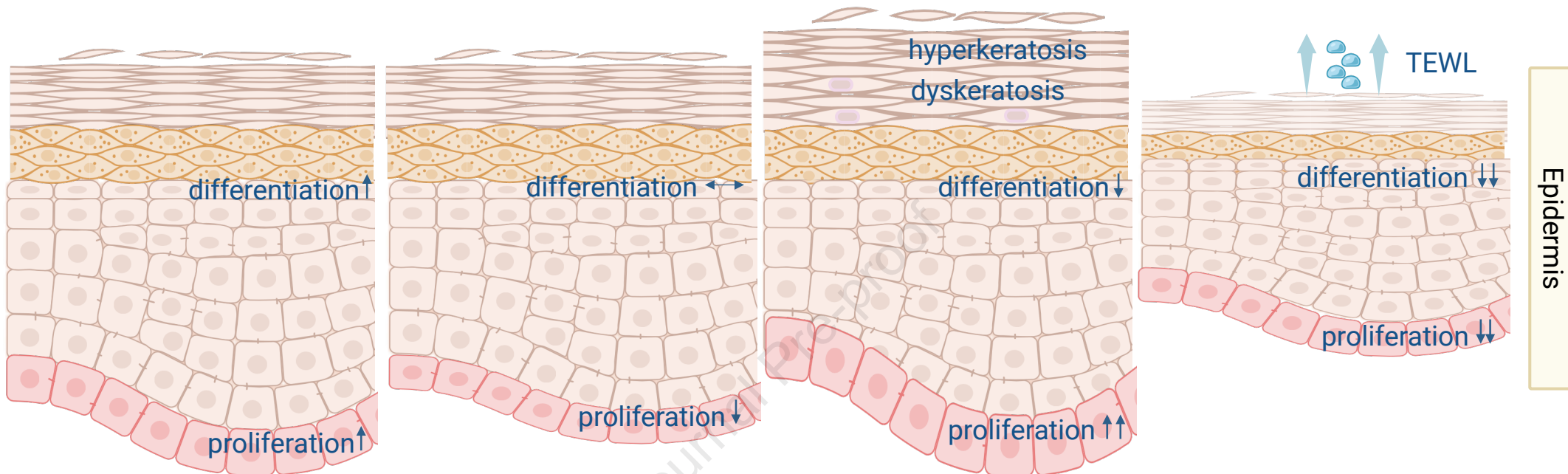
Please cite this article as: Boix J, Knuever J, Niehoff N, Sen A, Pla-Martin D, Baris OR, Etich J, Brachvogel B, Kaul H, Isbrandt D, Soroka E, Bazzi H, Wenger RH, Giavalisco P, Wiesner RJ, Constitutive HIF-1 α expression in the epidermis fuels proliferation and is essential for effective barrier formation, *The Journal of Investigative Dermatology* (2024), doi: <https://doi.org/10.1016/j.jid.2024.09.022>.

This is a PDF file of an article that has undergone enhancements after acceptance, such as the addition of a cover page and metadata, and formatting for readability, but it is not yet the definitive version of record. This version will undergo additional copyediting, typesetting and review before it is published in its final form, but we are providing this version to give early visibility of the article. Please note that, during the production process, errors may be discovered which could affect the content, and all legal disclaimers that apply to the journal pertain.



Metabolic regulation of neonatal epidermis composition

Journal Pre-proof

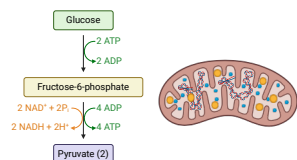


Metabolic homeostasis

Glycolysis ↓↓ (OxPhos ↑)

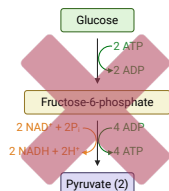
OxPhos ↓↓ (Glycolysis ↑)

OxPhos ↓↓ & Glycolysis ↓↓



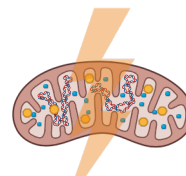
control

set-up of intact skin barrier



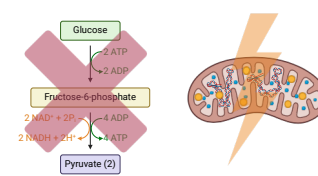
HIF^{eko}

compensated normal construction of epidermis



Twinkle^{epi}

skin inflammation & systemic lactic acidosis



TwinkleHIF^{epi}

severe barrier defect & systemic inflammation

Epidermis

Constitutive HIF-1 α expression in the epidermis fuels proliferation and is essential for effective barrier formation

Julia Boix^{1,2*}, Jana Knuever^{1,3*}, Nadine Niehoff¹, Ayesha Sen¹, David Pla-Martin^{1,2,4}, Olivier R. Baris⁵, Julia Etich⁶, Bent Brachvogel^{2,6,7}, Harshita Kaul⁷, Dirk Isbrandt^{2,8,9}, Ekaterina Soroka^{3,7}, Hisham Bazzi^{2,3,7}, Roland H. Wenger¹⁰, Patrick Giavalisco¹¹ and Rudolf J. Wiesner^{1,2,7}

¹Center for Physiology and Pathophysiology, Institute of Systems Physiology, University of Köln, Germany

²Center for Molecular Medicine Cologne, University of Köln, Germany

³Department of Dermatology and Venereology, University Hospital of Köln, Köln, Germany

⁴Institute of Biochemistry and Molecular Biology I, University Hospital Düsseldorf - Heinrich Heine University, Düsseldorf, Germany

⁵University of Angers, MitoLab, Unité MITOVASC, UMR CNRS 6015, INSERM U1083, SFR ICAT, Angers, France

⁶Department of Pediatrics and Adolescent Medicine, Experimental Neonatology, Faculty of Medicine and University Hospital Cologne, University of Cologne, Cologne, Germany.

⁷Cologne Excellence Cluster on Cellular Stress Responses in Aging-associated Diseases (CECAD), University of Köln, Germany

⁸Institute for Molecular and Behavioral Neuroscience, Faculty of Medicine, University of Köln, Germany

⁹German Center for Neurodegenerative Diseases (DZNE), Bonn, Germany

¹⁰Institute of Physiology, University of Zurich, Zurich, Switzerland

¹¹Max Planck Institute for Biology of Aging, Cologne, Germany

Corresponding author: Dr. Jana Knuever, MD, jana.knuever@uk-koeln.de

* Julia Boix and Jana Knuever contributed equally

Abstract

Epidermis is one of the most rapidly proliferating tissues in the body with high demands for ATP and cellular building blocks. Here we show that, in order to meet these requirements, keratinocytes constitutively express hypoxia-inducible factor-1 α (HIF-1 α), even in the presence of oxygen levels sufficient for HIF-1 α hydroxylation. We previously reported that mice with severe epidermal mitochondrial dysfunction actually showed a hyperproliferative epidermis, but rapidly died of systemic lactic acidosis and hypoglycemia, indicating excessive glycolysis. In the present work, we interrogated HIF-1 α function in glycolysis by its epidermal ablation combined with mitochondrial dysfunction, which resulted in decreased proliferation but even earlier lethality due to a severe barrier defect. Our data demonstrate that HIF-1 α is indispensable for maintaining a high aerobic glycolytic flux necessary for supplying energy, but also for synthesizing cellular building blocks like lipids, which are both essential for proliferation as well as barrier formation. HIF-1 α is stabilized in keratinocytes in the presence of oxygen by high levels of HIF-1 α transcripts, low levels of prolyl-4-hydroxylases (PHD2 and 3) and a low cellular α -ketoglutarate/lactate ratio, likely inhibiting PHD activity. Our data suggest a key role for constitutive HIF-1 α expression allowing a Warburg-like metabolism in healthy, highly proliferative keratinocytes, similar to tumour cells.

Keywords

epidermal barrier function / HIF-1 α / lipid synthesis / mitochondrial DNA / skin homeostasis

Introduction

Oxygen levels vary among tissues, and can be very low in wounds and in solid tumors. Most, if not all cells in the body react to hypoxia by stabilizing hypoxia-inducible transcription factors HIF-1 α and/or HIF-2 α to cope with an interruption of oxygen supply and restore tissue homeostasis. HIF α subunits are marked for proteasomal degradation by oxygen and α -ketoglutarate dependent prolyl-4-hydroxylase domain (PHD) enzymes (Schofield and Ratcliffe, 2004). HIF-1, among many other functions, activates a gene expression program that readjusts cellular metabolism with high rates of anaerobic glycolysis, suppressed oxidative phosphorylation (OXPHOS) and stimulated angiogenesis (Fuhrmann and Brüne, 2017). Thus, HIF-1 ultimately serves as the master regulator of energy homeostasis (Semenza, 2009) (Semenza, 2012). HIF-1 α protein is constitutively expressed in the basal layer of normal human (Rezvani H. R. et al., 2011) and mouse epidermis (Boutin et al., 2008), also reviewed in (Rezvani Hamid R et al., 2011). It was claimed that this is due to physiologic hypoxia in the epidermis (Evans et al., 2006), and that skin thus senses environmental hypoxia and contributes to renal erythropoietin production (Boutin et al., 2008). Low oxygen partial pressure (pO₂) in the environmental air is, however, a condition rarely encountered by mammals and therefore this hypothesis was severely questioned (Paus et al., 2009). Rasmussen and colleagues later demonstrated that following exposure of human subjects to either systemic or skin hypoxia, the skin does not contribute to erythropoietin expression (Rasmussen et al., 2012). In addition, pO₂ is not particularly low in skin (reviewed in (Keeley and Mann, 2019)) and no hypoxic region was detected in the epidermis using penetrating oxygen electrodes (Baumgärtl et al., 1987), further questioning both the mechanism and the role for constitutive HIF-1 α stabilization. Indeed, no obvious skin phenotype was reported in HIF^{eko} mice (Boutin et al., 2008), and only after six months moderate skin atrophy and pruritic inflammation were observed with dysregulation of several basal lamina proteins (Rezvani H. R. et al., 2011). In addition, it was shown that in the absence of HIF-1 α , tissue damage upon UVB irradiation is aggravated (Faßbender et al., 2022). Also, ablation of HIF-1 α in the epidermis prevents tumorigenesis but at the same time triggers the formation of hyperkeratotic plaques in later life of mice (Mahfouf et al., 2019). Finally, bacterial infection-induced hypoxia drives increased glutamine metabolism in keratinocytes with attendant enhancement of skin and hair follicle regeneration (Wang et al., 2023).

The epidermis is one of the most rapidly proliferating normal tissues in the body. Dividing and differentiating keratinocytes require a constant supply of energy and building material in order to produce cellular building blocks. Our previous studies have shown that keratinocytes in the basal epidermal layer are rich in mitochondria (Hornig-Do et al., 2007) (Knuever et al., 2012), but others proposed that epidermal energy metabolism is functionally anaerobic, based on high lactate production of epidermal sheets, which is not further increased under hypoxia (Ronquist et al., 2003). Therefore, ATP production may not be the only reason for the high mitochondrial content in the basal layer, but also the synthesis of pyrimidine nucleotides and membrane lipids for daughter cells, less well-known but essential mitochondrial functions (Wallace, 2012). Consequently, we previously studied mitochondrial function in the epidermis by genetically interfering with mitochondrial DNA (mtDNA) transcription (TFAM^{eko} mice) (Baris et al., 2011) or mtDNA replication in mice expressing the dominant-negative mutant K320E of the mitochondrial helicase Twinkle (K320E-Twinkle^{epi} mice) (Weiland et al., 2018). We observed no major differentiation defects in the absence of the OXPHOS system, but disturbed development of ectodermal appendages, such as hair follicles, sebaceous glands (Kloepper et al., 2015) or teeth pulps (Imhof et al., 2020), which have even higher biomass production rates. Although OXPHOS was absent in K320E-Twinkle^{epi} epidermis, a hyperproliferation of keratinocytes was observed, accompanied by a delay in barrier maturation. Animals died within one week after birth, due to a complex combination of factors, including high lactate levels in blood, hypoglycemia and increased expression of pro-inflammatory cytokines (Weiland et al., 2018). Interestingly, upregulation of *Hif1a* gene expression and HIF-1 target genes was observed in the mutant epidermis.

To reveal the role of HIF-1 α in epidermal homeostasis, we challenged its function by ablating *Hif1a* in K320E-Twinkle^{epi} mice (called TwinkleHIF^{epi} mice). These animals died even earlier due to severely disturbed lipid deposition with a profound barrier defect followed by an aggravated inflammatory phenotype. Thus, constitutively expressed HIF-1 α is not only necessary for the Warburg-like aerobic-glycolytic energy metabolism of the highly proliferative keratinocytes, similar to tumor cells, but also contributes to the formation of a competent epidermal barrier.

We find that HIF-1 α is stabilized in the epidermis by high expression levels of the *Hif1a* gene, low levels of PHD2/3 and a low intracellular α -ketoglutarate/lactate ratio, which further inhibits the capacity of PHDs for HIF-1 α degradation.

Results

HIF-1 α is highly expressed in the well-oxygenated epidermis as well as in cultured keratinocytes.

In vivo measurements of local pO₂ in normal mouse skin demonstrated values no lower than 30 Torr in the dermis (40 ± 10 Torr) and, most importantly, no hypoxic zone was observed in the epidermis (Figure 1a). *Hif1a* mRNA levels were 20-fold higher in mouse epidermis compared to the dermis (Figure 1b), and the protein was readily detectable in keratinocytes, even when a high pericellular pO₂ was ensured by cultivation of primary cells on plates with gas permeable bottoms (Figure 1c) (Wenger et al., 2015). HIF-1 α levels further increased under hypoxia and also upon increasing cell density, which decreases O₂ availability (Figure 1c; (Cho et al., 2008)). Therefore, constitutive expression of the generally highly unstable HIF-1 α protein in keratinocytes is not due to a hypoxic environment.

TwinkleHIF^{epi} mice die immediately after birth, although low lactate and high glucose levels are restored in the absence of HIF-1 α .

To understand the role of HIF-1 α in epidermal metabolism, we generated *Hif1a* knock-out mice in a background of mitochondrial dysfunction. All animal experiments were approved by the animal care committee of the University of Cologne and local government authorities (Bezirksregierung Köln; Landesamt für Natur, Umwelt und Verbraucherschutz [LANUV], Recklinghausen; Az.81-02.04.2019.A101; 84-02.04.2015.A405). Successful knock-out was confirmed by RT-qPCR and immunoblotting (Figures S1a, b). TwinkleHIF^{epi} mice were born in expected Mendelian ratios, but died at postnatal (P) day 0-1, while Twinkle^{epi} mice lived until P5–P8. Mice with an epidermal ablation of *Hif1a* alone (HIF^{eko} mice) survived like controls (Figure 2a). As observed before, expression of K320E-Twinkle in TwinkleHIF^{epi} mice resulted in a 5-fold decrease of mtDNA copy number and 10-fold decrease of a representative mtDNA encoded mRNA (mtCo3), leading to decreased levels of subunits representing the four OXPHOS complexes containing mtDNA encoded subunits (complex II containing no such subunits; Figures S1c-e). Complex I to IV remained normal in HIF^{eko} mice (Figure S2b-d), showing that constitutively expressed HIF-1 α does not suppress mitochondrial biogenesis in the epidermis, as observed in other cell types (Fuhrmann and Brüne, 2017).

However, the severe hypoglycemia and increased blood lactate levels already present at birth (Figures 2b, c) caused by mitochondrial dysfunction in *Twinkle^{epi}* mice (for later time points, see Weiland et al., 2018) were normalized in *TwinkleHIF^{epi}* mice, indicating that factors additional to lactic acidosis contribute to their short life span. Lactate and pyruvate levels in fresh frozen epidermal tissue were similar in all genotypes, indicating rapid removal of lactate into the systemic blood stream. Low levels of the glycolytic intermediates glucose-6-phosphate (G-6-P), fructose-6-phosphate (F-6-P) and fructose-1,6-bisphosphate (F-1,6-P₂) in epidermal tissue of *Twinkle^{epi}* mice are consistent with and mirror the increased glycolytic flux, while rather normal levels in *TwinkleHIF^{epi}* mice confirm the hampered flux in the absence of HIF-1 α . High steady state levels of phosphoenol-pyruvate (PEP) in both genotypes with defective mitochondria are probably due to low levels of fructose-1,6-bisphosphate, a potent activator of pyruvate kinase (see textbooks of biochemistry). *HIF^{eko}* mice presented blood lactate levels similar to controls. Notably, *Twinkle^{epi}* mice expressed 3-times more *Hif1a* mRNA compared to controls, but also mRNA levels of HIF-1 targets crucial for glucose metabolism were increased, including pyruvate dehydrogenase kinase 4 (*Pdk4*, 4.7fold), hexokinase 2 (*Hk2*, 2.1fold) and the glucose transporter 1 (*Glut1/Slc2a1*; 1.5fold) (Figure 2d). These data suggest that epidermis in *Twinkle^{epi}* mice adapts to the OXPHOS defect by augmentation of *Hif1a* gene expression followed by downstream key glycolysis genes as HIF targets, which however leads to fatal systemic lactic acidosis. In *TwinkleHIF^{epi}* mice, the expression of all three genes was considerably lower than in *Twinkle^{epi}* newborns (0.8fold, 0.6fold, and 0.7fold, respectively) and *Hk2* and *Slc2a1* mRNA was even lower than controls, showing that constitutively stabilized HIF-1 α is essential for maintaining the normal epidermal aerobic-glycolytic program. Significantly low levels of *Slc2a1* mRNA in *HIF^{eko}* mice support this findings. *Twinkle^{epi}* mice also showed upregulation of neovascularization genes such as adrenomedullin (*Adm*, 9.9fold) and vascular endothelial growth factor A (*Vegfa*, 2.7fold), but their expression was normalized to control levels in the absence of HIF-1 α (Figure 2e), further supporting HIF-1 α activation in the absence of functional mitochondria.

The aerobic-glycolytic phenotype of the epidermis was confirmed by measuring the extracellular acidification rate (ECAR; proportional to lactate production, Figure S3a). Although they proliferate slower *in vitro* when compared to fibroblasts, *wild-type* keratinocytes produced 3x more lactate and consumed 75% more oxygen,

consequently showing a 75% higher rate of ATP production by OXPHOS (Figures S3b-f). In summary, these data confirm that constitutively stabilized HIF-1 α is essential for maintaining an aerobic-glycolytic metabolism of the epidermis. Upon OXPHOS impairment, upregulation of *Hif1a* followed by HIF-1 target genes activate compensatory mechanisms to maintain energy homeostasis.

Proliferation and differentiation are impaired in TwinkleHIF^{epi} mice.

Histologically, no major skin differentiation defects were observed in all mutant mice at birth (Figure 3). Also dermal thickness was similar in all strains (Figure S4a). However, the basal proliferative layer showed a significant reduction in the number of Ki67-positive keratinocytes in the TwinkleHIF^{epi} double mutant as well as in the HIF^{eko} mice (Figure 3b), leading to a 50% decrease in total epidermal thickness (Figure 3a). Twinkle^{epi} showed no differences to controls in epidermal thickness or keratinocyte proliferation, but HIF^{eko} presented levels similar to TwinkleHIF^{epi} mice. Keratin 14 and keratin 10 intensity was reduced in Twinkle^{epi} and TwinkleHIF^{epi} mice (Figure 3c, d). Staining for loricrin (Figure 3e) was reduced in TwinkleHIF^{epi} mice, while filaggrin staining intensity was similar in all genotypes (Figure S4c). The early proliferation defect in HIF^{eko} mice was compensated later, since adult mice had normal epidermal thickness (Figure S4b).

In stark contrast, Twinkle^{epi} keratinocytes even proliferate faster, probably fueled by activating aerobic glycolysis upon OXPHOS impairment (Figure 3b; for later time points see (Weiland et al., 2018), leading to enhanced epidermal thickness (Figure 3a). Caspase-3 positive cells were observed only in HIF^{eko} mice (Figure S5c, e).

These data suggest that constitutive HIF-1 α expression is mandatory to maintain a sufficiently high production rate of ATP and of cellular building blocks for epidermal proliferation and survival, while a mitochondrial defect in the presence of HIF-1 α can be compensated.

TwinkleHIF^{epi} mice show an epidermal maturation delay and a severe barrier defect.

TwinkleHIF^{epi} mice exhibited small lesions or even wounds in the ventral skin at birth (Figure 4a), suggesting skin fragility, probably induced by mechanical stress upon birth, since such lesions were absent in late embryos. Using toluidine blue, we investigated if barrier integrity was generally impaired. At P0, no general penetration

of the dye was observed in skin of controls, while lesions were naturally stained in TwinkleHIF^{epi} mice (Figure 4b). At E17.5, toluidine blue penetration was noted in the entire TwinkleHIF^{epi} ventral skin but not in controls, indicating a delay in epidermal maturation. The same assay revealed only a mild maturation delay in Twinkle^{epi} mice, which was completely resolved at birth (Weiland et al., 2018).

TwinkleHIF^{epi} mice showed a 2.2-fold increase in transepidermal water loss (TEWL, Figure 4c) and a significant reduction in body weight compared to all other strains (Figure 4d), indicating a severe disruption of the inside-out barrier function as well. A proper epidermal barrier is mainly supported by a network of keratins and cornified envelope proteins such as filaggrin, loricrin or small proline rich proteins (SPRRs), tight junctions (containing claudins), as well as lipids (ceramides, free fatty acids and cholesterol) which together build the *stratum corneum* (Segre, 2006, van Smeden and Bouwstra, 2016). Probably as a compensatory response, *Sprr2d*, *Sprr2h* and *Cldn4* mRNAs were highly increased in TwinkleHIF^{epi} epidermis (13.6-, 5.9- and 4.0-fold, respectively), but less in Twinkle^{epi} compared to controls or HIF^{eko} mice (Figure 4e). Nonetheless, upregulation of these epidermal differentiation cluster genes failed to compensate the severe barrier defect when HIF-1 α and functional mitochondria were absent.

Both functional mitochondria and HIF-1 α are required for proper lipid deposition.

Nile-red staining of polar (red) and non-polar lipids (green) showed that while all *stratum corneum* layers mainly contain polar lipids in control and Twinkle^{epi} mice, their content was significantly reduced in HIF^{eko} and TwinkleHIF^{epi} mice (Figures 5a, b). This demonstrates a severe defect in the synthesis and/or deposition of polar lipids in the absence of HIF-1 α and/or dysfunctional mitochondria. Hence, we analyzed the expression of the key enzymes in the synthesis pathways of the three main polar lipid classes of the *stratum corneum* (Figure 5c): elongation of very long chain fatty acids protein 3 (*Elovl3*), phospholipase A2 group V (*Pla2g5*) and cathepsin E (*Ctse*) (Segre, 2006; Pappas, 2009). In agreement with our staining results, *Elovl3* mRNA was decreased in the epidermis of Twinkle^{epi} and TwinkleHIF^{epi} by approximately 75%, *Pla2g5* was downregulated by 40% and 75%, respectively, while the decrease in *Ctse* expression was not significant. Expression of filaggrin (*Flg*) mRNA, a key protein for proper *stratum corneum* function, was reduced in TwinkleHIF^{epi} mice only. This result

was not corroborated by filaggrin protein staining (Figure S4c). HIF^{eko} mice did not show differences related to controls (Figure 5c, S4c).

Since mTORC2 was shown to control lipid synthesis as well as filaggrin processing during epidermal barrier formation (Ding et al., 2020), we analyzed expression of rictor, an adaptor protein in the mTORC2 complex, which was downregulated in TwinkleHIF^{epi} mice compared to controls (Figure 5c). Moreover, mTORC2 complex activity, analyzed by the pAKT/AKT ratio, was clearly lower in TwinkleHIF^{epi} mice at birth compared to controls (Figures 5d, e), possibly contributing to the metabolic disability of the epidermis forming a functioning barrier and lipophilic *stratum corneum*. In summary, our data indicate that both, proper mitochondrial function and HIF-1 α activity, are important for adequate expression of enzymes involved in cornified envelope formation, especially in lipid synthesis.

The inflammatory response induced by mitochondrial dysfunction is exaggerated in the absence of HIF-1 α .

The inflammatory skin phenotype of Twinkle^{epi} mice was due to an increased expression of pro-inflammatory genes, possibly explained by a release of mitochondrial DAMPs a few days after birth (Weiland et al., 2018). In TwinkleHIF^{epi} mice, the expression of pro-inflammatory genes was further exacerbated shortly after birth (Figure S5a, note the log scale). While expression of interleukin 1 beta (*Il1b*) and nitric oxide synthase 2 (*Nos2*) were comparable to controls in Twinkle^{epi} mice, TwinkleHIF^{epi} mice showed a 9.9- and 7.8-fold increase, respectively. The expression of S100 calcium binding protein A8 and A9 (*S100a8*, *S100a9*) and secretory leukocyte peptidase inhibitor (*Sipi*) dramatically increased up to 45-, 34- and 28-times in TwinkleHIF^{epi} mice, respectively. Expression of wounding-associated keratin 6b (*K6b*) and tumour necrosis factor (*Tnfa*) was also augmented in TwinkleHIF^{epi} mice (Figure S5a), while the absence of HIF-1 α alone in HIF^{eko} mice had no effect on the expression of all these genes. *Il6* mRNA was undetectable in epidermis of all four genotypes (data not shown), but the IL-6 cytokine was found at high levels in serum of TwinkleHIF^{epi} mice (Figure S5b), showing that the severe barrier defect has caused a systemic response. However, numbers of macrophages (F4/80) and mast cells (Giemsa) were comparable in all four genotypes (Figures S5c, d), indicating that, at birth, an immune cell infiltrate had not yet been recruited. These data indicate that

epidermal and systemic inflammation may contribute to the very early death of TwinkleHIF^{epi} mice and is caused by the severe barrier defect.

How is HIF-1 α constitutively stabilized under normoxic conditions?

Under normoxia, HIF-1 α is hydroxylated by PHDs, and degraded by the proteasome (Schofield and Ratcliffe, 2004), while at low oxygen availability, PHD activity is inhibited and consequently HIF-1 α is stabilized. However, other factors and metabolites additionally modulate PHD function, allowing for HIF-1 α stabilization independent of oxygen (Fuhrmann and Brüne, 2017) (Semenza, 2012).

We thus first hypothesized that HIF-1 α stabilization was related to high reactive oxygen species (ROS) levels present in human keratinocytes (Hornig-Do et al., 2007), because ROS have recently been shown to oxidatively inactivate PHDs (Lee et al., 2020). Hence, we incubated keratinocytes with trolox and N-acetylcystein, two powerful ROS scavengers (Cordes et al., 2009) (Aldini et al., 2018) (Deneke, 2001) (Kitasaka et al., 2020), but observed no relevant effect, neither on HIF-1 α protein or mRNA levels, nor on expression of HIF-1 target genes (Figures S6a, b).

On the other hand, levels of the HIF-1 α degrading enzymes PHD2 and PHD3 were lower in *wild-type* keratinocytes compared to fibroblasts (Figure 6a, b). In addition, HIF-1 α stabilization independent of oxygen availability was also demonstrated in cells with high intracellular levels of the tricarboxylic acid (TCA) cycle metabolites fumarate and succinate and its by-product 2-OH-glutarate (2-OH-G). Since α -ketoglutarate (α -KG) is necessary for PHDs while the other metabolites are inhibiting, we calculated ratios of α -KG/inhibiting metabolites, assuming that ratios below 1 will inhibit PHDs and stabilize HIF-1 α , as shown before (Ryan et al., 2019, Williams et al., 2022, Yogev et al., 2010). The ratios were as follows: α -KG/succinate, 1.82; α -KG/fumarate, 1.17; and α -KG/2-OH-G, 5.04 (Figure 6c, left panel). However, the ratio of α -KG/lactate was 0.14, making the extremely high intracellular lactate concentration a possible candidate. Together with low α -KG/fumarate (0.73) and low α -KG/lactate (0.30) ratios in fresh frozen epidermis (Figure 6c, right panel), we propose that high intracellular lactate and possibly fumarate, together with low levels of PHDs and in combination with high *Hif1a* mRNA (Figure 1b) are responsible for the constitutive epidermal expression of HIF-1 α in the presence of oxygen.

Discussion

We found that the highly unstable transcription factor HIF-1 α is constitutively expressed in keratinocytes even in the presence of oxygen. In fact, a high steady-state oxygen level in the epidermis *in vivo* is maintained by oxygen flux from dermal blood vessels, located close to the basement membrane, as well as by oxygen supply from the surrounding air (Stücker et al., 2002, Stücker et al., 2000).

Using three mouse models, we demonstrate that HIF-1 α expression in the epidermis is required for maintaining a constitutively high aerobic-glycolytic flux. When absent in TwinkleHIF^{epi} and HIF^{eko} epidermis, low expression of the glucose transporter Slc2a1 and of important glycolysis-related target genes, respectively, indicates that the HIF transcription factor is crucial for basal glycolysis gene expression. A high glycolytic flux in the presence of oxygen may be necessary for the high proliferation rate of the basal layer providing ATP, but also cellular building blocks, comparable to the Warburg effect observed in many tumor cells with a similar expression profile of metabolic genes (Kierans and Taylor, 2021).

Additionally, we show that HIF-1 α establishes a potentially compensatory mechanism in the epidermis upon OXPHOS impairment, which occurs in sun-exposed skin areas especially vulnerable to extrinsic aging (Birket and Birch-Machin, 2007, Hudson et al., 2016), and which are due to the accumulation of mtDNA deletions and point mutations. Twinkle^{epi} mice even showed increased keratinocyte proliferation leading to increased epidermal thickness. In stark contrast, in TwinkleHIF^{epi} mice, with the same severe mitochondrial defect, the absence of HIF-1 α prevented the increase in glycolytic flux necessary to compensate for the OXPHOS defect. This results in diminished keratinocyte proliferation and, consequently, reduction in epidermal thickness. In agreement, hyperproliferative keratinocytes from psoriatic lesions express high levels of HIF (Rosenberger, 2007) and human *HIF1 α* knock-down keratinocytes were not able to form a stratified epidermis *in vitro* and showed reduced proliferation (Rezvani H. R. et al., 2011).

The metabolic defect in TwinkleHIF^{epi} mice causes a delay in epidermal outside-in barrier maturation at E17.5. The induced expression of *Spr2d*, and *Spr2h* at birth in both Twinkle^{epi} and TwinkleHIF^{epi} mouse models is similar to the compensatory mechanism promoting a functional barrier described in loricrin epidermal knock-out mice (Huebner et al., 2012). In both genotypes, the outside-in barrier was fully

functional at birth except for small ventral lesions found in TwinkleHIF^{epi} mice due to skin fragility. However, the inside-out barrier was severely disturbed in TwinkleHIF^{epi} mice as shown by an impressive water resulting in weight loss, likely one cause of early death. Our findings are similar to other reported mouse models of disrupted epidermal barrier, e.g. HIF-1 β epidermal knock-out mice showing an impaired barrier and postnatal death due to severe dehydration (Takagi et al., 2003).

Decreased deposition of polar lipids may significantly contribute to the inside-out barrier defect in TwinkleHIF^{epi} mice, similar to mice that are deficient in epidermal lipid synthesis enzymes (Pappas, 2009, Segre, 2006). Surprisingly, mitochondrial dysfunction not only causes defective lipid synthesis, as expected, but also reduced expression of enzymes important for the *de novo* synthesis of barrier lipids (*Elovl3* and *Pla2g5*). In Twinkle^{epi} mice, lipid deposition was not impaired despite downregulation of *Elovl3* and *Pla2g5* mRNAs. HIF^{eko} newborns showed decreased polar lipid deposition but no differences in the expression of lipid synthesis related genes. We propose that the impairment of both OXPHOS and aerobic glycolysis in TwinkleHIF^{epi} mice leads to compensatory downregulation of these essential genes in order to reduce the metabolic load of synthesizing extracellular lipids.

As expected, impairment of ATP production in TwinkleHIF^{epi} mice led to mTORC2 inhibition with downregulation of *Rictor* expression and a lower activation state of AKT by phosphorylation (Ser473). Accordingly, the skin phenotype of epidermal *Rictor* knock-out mice (Ding et al., 2020) shares many similarities with that of TwinkleHIF^{epi} mice at birth, including reduced keratinocyte proliferation, epidermal thinning, diminished lipid synthesis and deposition, increased TEWL, delayed epidermal barrier maturation, and increased pro-inflammatory cytokine expression. In Twinkle^{epi} mice with augmented glycolytic flux neither downregulation of *Rictor* nor diminished AKT activation was observed, also explaining the absence of a barrier defect.

Cytokine induction and inflammation are intrinsic responses to epidermal barrier disruption (Segre, 2006). Skin has been shown to be an important source of systemic cytokines during aging (Hu et al., 2017), when a functional epidermal barrier is compromised due to defective repair mechanisms (Velarde, 2017). Local and systemic cytokine induction, but not epidermal hyperplasia, was detected in TwinkleHIF^{epi} mice at birth, most likely due to the loss of HIF-1 α and its effect on keratinocyte proliferation, as described *in vitro* (Rezvani H. R. et al., 2011). In conclusion, both the severe

epidermal barrier dysfunction and the induction of pro-inflammatory cytokines probably lead to the premature death of TwinkleHIF^{epi} mice.

Finally, factors others than hypoxia are obviously responsible for epidermal HIF-1 α stabilization and even in hypoxia, HIF-1 α stabilization is mostly not oxidant-initiated, as recent findings have shown (Kumar et al., 2021). We find that ROS, altered by ROS scavenger treatment *in vitro*, neither impact *Hif1a* mRNA nor HIF-1 α protein levels in keratinocytes. Succinate, fumarate and 2-OH-glutarate do not reach levels high enough to inhibit PHDs, when related to their substrate α -ketoglutarate. However, low levels of PHD2 and PHD3 as well as high intracellular lactate may importantly contribute to normoxic HIF-1 α stabilization, as previously described (De Saedeleer et al., 2012).

In summary, the metabolic defects seen upon OXPHOS dysfunction in the epidermis are more severe in the absence of HIF-1 α , indicating that HIF-1 α is necessary for maintaining its basal metabolic phenotype. Our data suggest a novel role for HIF-1 α as a guardian of epidermal homeostasis through regulation of keratinocyte aerobic-glycolytic energy metabolism, but, equally important, also anabolic reactions necessary for cell division and synthesis of barrier lipids.

Materials and Methods

Oxygen partial pressure in skin *in vivo*

The local pO₂ in mouse skin was determined using a Clark-type oxygen microelectrode with a tip diameter of 10 μ m (Unisense, Copenhagen, Denmark) on 3 consecutive locations on the shaved scalp of three anesthetized mice (1-1.5% isoflurane in 100% oxygen). Mice were kept at 37°C on a homeothermic heating pad with intraauricular fixation in a stereotaxic apparatus (Stoelting, Dublin, Ireland). To avoid oxygen convection into an air filled channel after skin penetration, the location was sealed with a drop of 0.9% NaCl solution. After calibration, the electrode was vertically moved forward into the skin in 10- μ m steps using a motorized, computer-controlled stereotaxic instrument (Neurostar, Tübingen, Germany), and pO₂ values were recorded each second. To demonstrate proper responsiveness of the electrode towards oxygen, the blood flow was increased with topically applied glycerol trinitrate (G. Pohl-Boskamp, Hohenlockstedt, Germany).

All animal experiments were approved by the animal care committee of the University of Cologne and local government authorities (Bezirksregierung Köln; Landesamt für Natur, Umwelt und Verbraucherschutz [LANUV], Recklinghausen; Az.81-02.04.2019.A101; 84-02.04.2015.A405).

All standard Materials and Methods are described in Suppl. Material.

Acknowledgements

J.B., J.K., A.S., H.B. and R.J.W. were supported by the Deutsche Forschungsgemeinschaft (DFG, German Research Foundation, Project-ID 73111208 - SFB 829/A14/A12/Z03 projects). J.E. and B.B. by DFG to the Research Unit FOR2722 - BR2304/12-1 - 407146744, ET144/3-2384170921 and to BR2304/7-1 – 207342459. H.B. and R.J.W. were also funded by the Cologne Excellence Cluster on Cellular Stress Responses in Aging-associated Diseases (CECAD). J.K. was supported by the Koeln Fortune Program, Faculty of Medicine, University of Cologne (465/2019 and 254/2022). O.R.B was supported by Agence Nationale de la Recherche (ANR-20-CE92-0020-01). The authors thank the CECAD Central Imaging Facility for support. We also acknowledge Prof. Bernhard Brüne and Dr. Nathalie Dehne, Institute of Biochemistry I, Frankfurt, for the gift of Hif1a^{loxP/loxP} mice. We are very grateful to PD Dr. Thomas Streichert, Sven Schmidt and Elke Dietzel, Institute for Clinical Chemistry, Cologne, for measuring glucose and lactate in our samples. We thank Max Schütter for his work in performing and analyzing metabolomics data and the Frezza lab (CECAD) for continuous discussion of our data and gift of reagents.

Author contributions

Investigation: JB, JK, DPM, AS, NN, PG. Formal analysis: JB, JK, DPM, PG. Project Administration: DI, ES, HB, JE, BB, ORB, RHW. Conceptualization and Supervision: RJW. Writing – original draft: JB, JK, RJW. Writing – review & editing: All authors.

Conflict of interest

The authors state no conflict of interest.

Data availability statement

All data supporting the conclusions of the manuscript are shown in the corresponding figures and supplements. No large datasets were generated or analyzed.

References

- Aldini G, Altomare A, Baron G, Vistoli G, Carini M, Borsani L, et al. N-Acetylcysteine as an antioxidant and disulphide breaking agent: the reasons why. *Free radical research* 2018;52(7):751-62.
- Baris OR, Klose A, Kloepper JE, Weiland D, Neuhaus JF, Schauen M, et al. The mitochondrial electron transport chain is dispensable for proliferation and differentiation of epidermal progenitor cells. *Stem Cells* 2011;29(9):1459-68.
- Baumgärtl H, Ehrly A, Saeger-Lorenz K, Lübbers D. Initial results of intracutaneous measurements of pO₂ profiles. *Clinical Oxygen Pressure Measurement: Tissue Oxygen Pressure and Transcutaneous Oxygen Pressure*: Springer; 1987. p. 121-8.
- Birket MJ, Birch-Machin MA. Ultraviolet radiation exposure accelerates the accumulation of the aging-dependent T414G mitochondrial DNA mutation in human skin. *Aging Cell* 2007;6(4):557-64.
- Boutin AT, Weidemann A, Fu Z, Mesropian L, Gradin K, Jamora C, et al. Epidermal sensing of oxygen is essential for systemic hypoxic response. *Cell* 2008;133(2):223-34.
- Cho Y-S, Bae J-M, Chun Y-S, Chung J-H, Jeon Y-K, Kim I-S, et al. HIF-1 α controls keratinocyte proliferation by up-regulating p21 (WAF1/Cip1). *Biochimica et Biophysica Acta (BBA)-Molecular Cell Research* 2008;1783(2):323-33.
- Cordes T, Vogelsang J, Tinnefeld P. On the mechanism of Trolox as antiblinking and antibleaching reagent. *Journal of the American Chemical Society* 2009;131(14):5018-9.
- De Saedeleer CJ, Copetti T, Porporato PE, Verrax J, Feron O, Sonveaux P. Lactate activates HIF-1 in oxidative but not in Warburg-phenotype human tumor cells. *PLoS One* 2012;7(10):e46571.
- Deneke SM. Thiol-based antioxidants. *Current topics in cellular regulation* 2001;36:151-80.
- Ding X, Willenborg S, Bloch W, Wickstrom SA, Wagle P, Brodesser S, et al. Epidermal mammalian target of rapamycin complex 2 controls lipid synthesis and filaggrin processing in epidermal barrier formation. *J Allergy Clin Immunol* 2020;145(1):283-300 e8.
- Evans SM, Schrlau AE, Chalian AA, Zhang P, Koch CJ. Oxygen levels in normal and previously irradiated human skin as assessed by EF5 binding. *Journal of Investigative Dermatology* 2006;126(12):2596-606.
- Faßbender S, Sondenheimer K, Majora M, Schindler J, Opitz FV, Pollet M, et al. Keratinocytes counteract UVB-induced immunosuppression in mice through HIF-1 α signaling. *Journal of Investigative Dermatology* 2022;142(4):1183-93.
- Fuhrmann DC, Brüne B. Mitochondrial composition and function under the control of hypoxia. *Redox Biol* 2017;Aug;12:208-215.
- Hornig-Do H-T, von Kleist-Retzow J-C, Lanz K, Wickenhauser C, Kudin AP, Kunz WS, et al. Human epidermal keratinocytes accumulate superoxide due to low activity of Mn-SOD, leading to mitochondrial functional impairment. *Journal of investigative dermatology* 2007;127(5):1084-93.
- Hu L, Mauro TM, Dang E, Man G, Zhang J, Lee D, et al. Epidermal dysfunction leads to an age-associated increase in levels of serum inflammatory cytokines. *Journal of Investigative Dermatology* 2017;137(6):1277-85.
- Hudson L, Bowman A, Rashdan E, Birch-Machin MA. Mitochondrial damage and ageing using skin as a model organ. *Maturitas* 2016;93:34-40.
- Huebner AJ, Dai D, Morasso M, Schmidt EE, Schafer M, Werner S, et al. Amniotic fluid activates the nrf2/keap1 pathway to repair an epidermal barrier defect in utero. *Dev Cell* 2012;23(6):1238-46.
- Imhof T, Rosenblatt K, Prymachuk G, Weiland D, Noetzel N, Deschner J, et al. Epithelial loss of mitochondrial oxidative phosphorylation leads to disturbed enamel and impaired dentin matrix formation in postnatal developed mouse incisor. *Scientific Reports* 2020;10(22037):77954-7.

- Keeley TP, Mann GE. Defining Physiological Normoxia for Improved Translation of Cell Physiology to Animal Models and Humans. *Physiol Rev* 2019;99(1):161-234.
- Kierans S, Taylor C. Regulation of glycolysis by the hypoxia-inducible factor (HIF): implications for cellular physiology. *The Journal of physiology* 2021;599(1):23-37.
- Kitasaka S, Yagi M, Kikuchi A. Suppression of menthyl anthranilate (UV-A sunscreen)-sensitized singlet oxygen generation by Trolox and, α -tocopherol. *Photochemical & Photobiological Sciences* 2020;19:913-9.
- Kloepper JE, Baris OR, Reuter K, Kobayashi K, Weiland D, Vidali S, et al. Mitochondrial function in murine skin epithelium is crucial for hair follicle morphogenesis and epithelial-mesenchymal interactions. *J Invest Dermatol* 2015;135(3):679-89.
- Knuever J, Poeggeler B, Gáspár E, Klinger M, Hellwig-Burgel T, Hardenbicker C, et al. Thyrotropin-releasing hormone controls mitochondrial biology in human epidermis. *The Journal of Clinical Endocrinology & Metabolism* 2012;97(3):978-86.
- Kumar A, Vaish M, Karuppagounder SS, Gazaryan I, Cave JW, Starkov AA, et al. HIF1 α stabilization in hypoxia is not oxidant-initiated. *Elife* 2021;Oct 1;10:e72873.
- Lee P, Chandel NS, Simon MC. Cellular adaptation to hypoxia through hypoxia inducible factors and beyond. *Nat Rev Mol Cell Biol* 2020;May;21(5):268-283.
- Mahfouf W, Hosseini M, Muzotte E, Serrano-Sanchez M, Dousset L, Moisan F, et al. Loss of epidermal HIF-1 α blocks UVB-induced tumorigenesis by affecting DNA repair capacity and oxidative stress. *Journal of Investigative Dermatology* 2019;139(9):2016-28. e7.
- Pappas A. Epidermal surface lipids. *Dermatoendocrinology* 2009((2)):72-6.
- Paus R, Bodó E, Kromminga A, Jelkmann W. Erythropoietin and the skin: a role for epidermal oxygen sensing? *Bioessays* 2009;31(3):344-8.
- Rasmussen P, Nordsborg N, Taudorf S, Sørensen H, Berg RM, Jacobs RA, et al. Brain and skin do not contribute to the systemic rise in erythropoietin during acute hypoxia in humans. *FASEB J* 2012;May;26(5):1831-4.
- Rezvani HR, Ali N, Nissen LJ, Harfouche G, De Verneuil H, Taïeb A, et al. HIF-1 α in epidermis: oxygen sensing, cutaneous angiogenesis, cancer, and non-cancer disorders. *Journal of Investigative Dermatology* 2011;131(9):1793-805.
- Rezvani HR, Ali N, Serrano-Sanchez M, Dubus P, Varon C, Ged C, et al. Loss of epidermal hypoxia-inducible factor-1 α accelerates epidermal aging and affects re-epithelialization in human and mouse. *J Cell Sci* 2011;124(Pt 24):4172-83.
- Ronquist G, Andersson A, Bendsoe N, Falck B. Human epidermal energy metabolism is functionally anaerobic. *Exp Dermatol* 2003;12(5):572-9.
- Rosenberger CS, C.; Rosenberger, A.D.; Jinping, L.; Treudler, R.; Frei, U.; Eckardt, K.U.; Brown, L.F. Upregulation of hypoxia-inducible factors in normal and psoriatic skin. *J Invest Dermatol* 2007;127(10):2445-52.
- Ryan DG, Murphy MP, Frezza C, Prag HA, Chouchani ET, O'Neill LA, et al. Coupling Krebs cycle metabolites to signalling in immunity and cancer. *Nat Metab* 2019;1:16-33.
- Schofield CJ, Ratcliffe PJ. Oxygen sensing by HIF hydroxylases. *Nat Rev Mol Cell Biol* 2004;May;5(5):343-54. .
- Segre JA. Epidermal barrier formation and recovery in skin disorders. *J Clin Invest* 2006;116(5):1150-8.
- Semenza GL. Regulation of oxygen homeostasis by hypoxia-inducible factor 1. *Physiology (Bethesda)* 2009;24:97-106.
- Semenza GL. Hypoxia-inducible factors in physiology and medicine. *Cell* 2012;Feb 3;148(3):399-408.
- Stücker M, Struk A, Altmeyer P, Herde M, Baumgärtl H, Lübbbers DW. The cutaneous uptake of atmospheric oxygen contributes significantly to the oxygen supply of human dermis and epidermis. *J Physiol* 2002;1(538):985-94.
- Stücker M, Struk A, Hoffmann K, Schulze L, Rochling A, Lübbbers DW. The transepidermal oxygen flux from the environment is in balance with the capillary oxygen supply. *J Invest Dermatol* 2000;114(3):533-40.

- Takagi S, Tojo H, Tomita S, Sano S, Itami S, Hara M, et al. Alteration of the 4-sphingene scaffolds of ceramides in keratinocyte-specific Arnt-deficient mice affects skin barrier function. *J Clin Invest* 2003;112(9):1372-82.
- van Smeden J, Bouwstra JA. Stratum Corneum Lipids: Their Role for the Skin Barrier Function in Healthy Subjects and Atopic Dermatitis Patients. *Curr Probl Dermatol* 2016;49:8-26.
- Velarde MC. Epidermal Barrier Protects against Age-Associated Systemic Inflammation. *J Invest Dermatol* 2017;137(6):1206-8.
- Wallace DC. Mitochondria and cancer. *Nat Rev Cancer* 2012;12(10):685-98.
- Wang G, Sweren E, Andrews W, Li Y, Chen J, Xue Y, et al. Commensal microbiome promotes hair follicle regeneration by inducing keratinocyte HIF-1 α signaling and glutamine metabolism. *Science Advances* 2023;9(1):eabo7555.
- Weiland D, Brachvogel B, Hornig-Do HT, Neuhaus JFG, Holzer T, Tobin DJ, et al. Imbalance of Mitochondrial Respiratory Chain Complexes in the Epidermis Induces Severe Skin Inflammation. *J Invest Dermatol* 2018;138(1):132-40.
- Wenger RH, Kurtcuoglu V, Scholz CC, Marti HH, Hoogewijs D. Frequently asked questions in hypoxia research. *Hypoxia* 2015;3:35-43.
- Williams NC, Ryan DG, Costa ASH, Mills EL, Jedrychowski MP, Cloonan SM, et al. Signaling metabolite L-2-hydroxyglutarate activates the transcription factor HIF-1 α in lipopolysaccharide-activated macrophages. *J Biol Chem* 2022;Feb;298(2):101501.
- Yogev O, Yogev O, Singer E, Shaulian E, Goldberg M, Fox TD, et al. Fumarase: A Mitochondrial Metabolic Enzyme and a Cytosolic/Nuclear Component of the DNA Damage Response. *Plos Biology* 2010;8(3):e1000328.

Figure Legends

Figure 1. HIF-1 α is highly expressed in the well-oxygenated epidermis as well as in cultured keratinocytes

(a) Representative graph of local pO₂ measured with a microelectrode inserted in vertical 10- μ m steps into mouse scalp skin. Epidermal and dermal layers are indicated, and an increase in pO₂ following NO-mediated vasodilation by glycerol trinitrate application is shown as positive control. (b) RT-qPCR showing *Hif1a* mRNA levels in epidermis (n=4) and dermis (n=3). Mean \pm standard deviation. Student's t-test; **, p-value < 0.01. (c) Immunoblot showing HIF-1 α protein in keratinocytes cultured with increasing density on normal and gas permeable plates. Keratinocytes cultured under hypoxic conditions (1% O₂, 6 h) served as positive control. β -Actin was used as loading control.

Figure 2. TwinkleHIF^{epi} mice die immediately after birth, although low lactate and high glucose levels are restored in the absence of HIF-1 α

(a) Graph showing the percentage of surviving control, HIF^{eko}, Twinkle^{epi} and TwinkleHIF^{epi} mice after birth (n=20-50 mice per genotype). (b) Blood glucose and

lactate (c) levels in control (n=24), HIF^{eko} (n=4), Twinkle^{epi} (n=17), and TwinkleHIF^{epi} (n=12) newborn mice. (d) Levels of glycolytic intermediates in fresh frozen epidermal tissue from control (n=4), Twinkle^{epi} (n=5) and TwinkleHIF^{epi} (n=6) newborn mice (no tissue was available for HIF^{eko} mice). (e) RT-qPCR showing *Hif1a*, *Pdk4*, *Hk2*, *Slc2a1*, and (f) *Adm* and *Vegfa* mRNA levels in control, HIF^{eko}, Twinkle^{epi} and TwinkleHIF^{epi} newborn epidermis at birth (n=3-8 mice per genotype). Mean ± standard deviation. One-way ANOVA, Tukey's post-hoc test; *, p-value < 0.05; **, p-value < 0.01; ***, p-value < 0.001.

Figure 3. Proliferation and differentiation are impaired in TwinkleHIF^{epi} mice

(a) Hematoxylin and eosin (H&E) staining and quantification of epidermal thickness, (b) immunostaining and quantification of Ki67-positive keratinocytes, bar = 50 μm, (c) immunostaining and quantification of keratin 14, (d) keratin 10 and (e) loricrin of control, HIF^{eko}, Twinkle^{epi} (n=3) and TwinkleHIF^{epi} newborn back skin at birth (n=4 mice per other three genotypes). (a, c-e) Bar = 200 μm. (a-e) Mean ± standard deviation. One-way ANOVA, Tukey's post-hoc test; *, p-value < 0.05; **, p-value < 0.01; ***, p-value < 0.001.

Figure 4. TwinkleHIF^{epi} mice show an epidermal maturation delay and a severe barrier defect

(a) Macroscopic ventral view of newborn control and TwinkleHIF^{epi} mice. (b) Toluidine blue staining (outside-in epidermal barrier function) at birth (P0) and embryonic day 17.5 (E) in control and TwinkleHIF^{epi} mice. (c) Transepidermal water loss (TEWL) assessment (inside-out epidermal barrier function) in control and TwinkleHIF^{epi} newborn mice (n=4-5 mice per genotype). (d) Control (n=36), HIF^{eko} (n=10), Twinkle^{epi} (n=10) and TwinkleHIF^{epi} (n=26) body weight at birth. (e) RT-qPCR showing *Sprr2d*, *Sprr2h*, *Ptgs2*, *Lor*, *Cldn1* and *Cldn4* mRNA levels in control, HIF^{eko}, Twinkle^{epi}, and TwinkleHIF^{epi} newborn epidermis (n=3-4 mice per genotype). (c-e) Mean ± standard deviation. (c) Student's t-test and (d, e) One-way ANOVA, Tukey's post-hoc test; *, p-value < 0.05; **, p-value < 0.01; ***, p-value < 0.001.

Figure 5. Both functional mitochondria and HIF-1α are required for proper lipid deposition

(a) Nile-red staining and (b) quantification of polar lipids in newborn control (n=5), HIF^{eko} (n=5), Twinkle^{epi} (n=3) and TwinkleHIF^{epi} skin (n=4); polar lipids (red), non-polar lipids (green), DAPI (blue). Scale bar = 100 μ m. (c) RT-qPCR showing *Elovl3*, *Pla2g5*, *Ctse*, *Flg* and *Rictor* mRNA levels in control, HIF^{eko}, Twinkle^{epi} and TwinkleHIF^{epi} newborn epidermis (n=3-4 mice per genotype). (d) Immunoblot of pAKT and AKT and (e) quantification in control, Twinkle^{epi} and TwinkleHIF^{epi} epidermal sheets (n=4 mice per genotype). (b, c, e) Mean \pm standard deviation. One-way ANOVA, Tukey's post-hoc test; *, p-value < 0.05; **, p-value < 0.01; ***, p-value < 0.001.

Figure 6. How is HIF-1 α constitutively stabilized under normoxic conditions?

(a) Representative immunoblot of PHD2 and PHD3 and quantification (b) in *wild-type* keratinocytes and fibroblasts. β -Actin and Ponceau S (PS) were used as loading controls. (c) Ratios of metabolites relevant for PHD activity in *wild-type* keratinocytes (left, n=4 biological replicates) and *wild-type* epidermal tissue (right, n=4 biological replicates). Mean \pm standard deviation. Student's t-test; *, p-value < 0.05; **, p-value < 0.01.

Figure 1

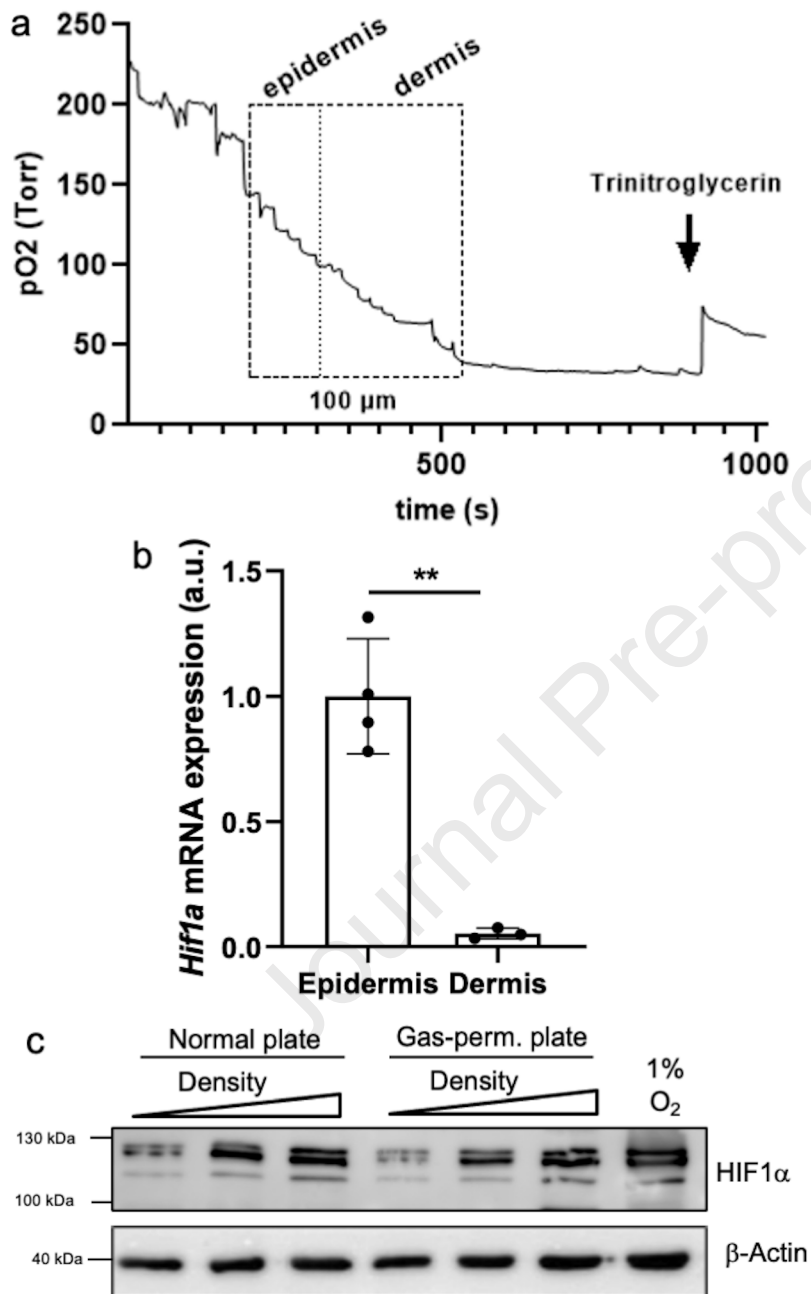


Figure 2

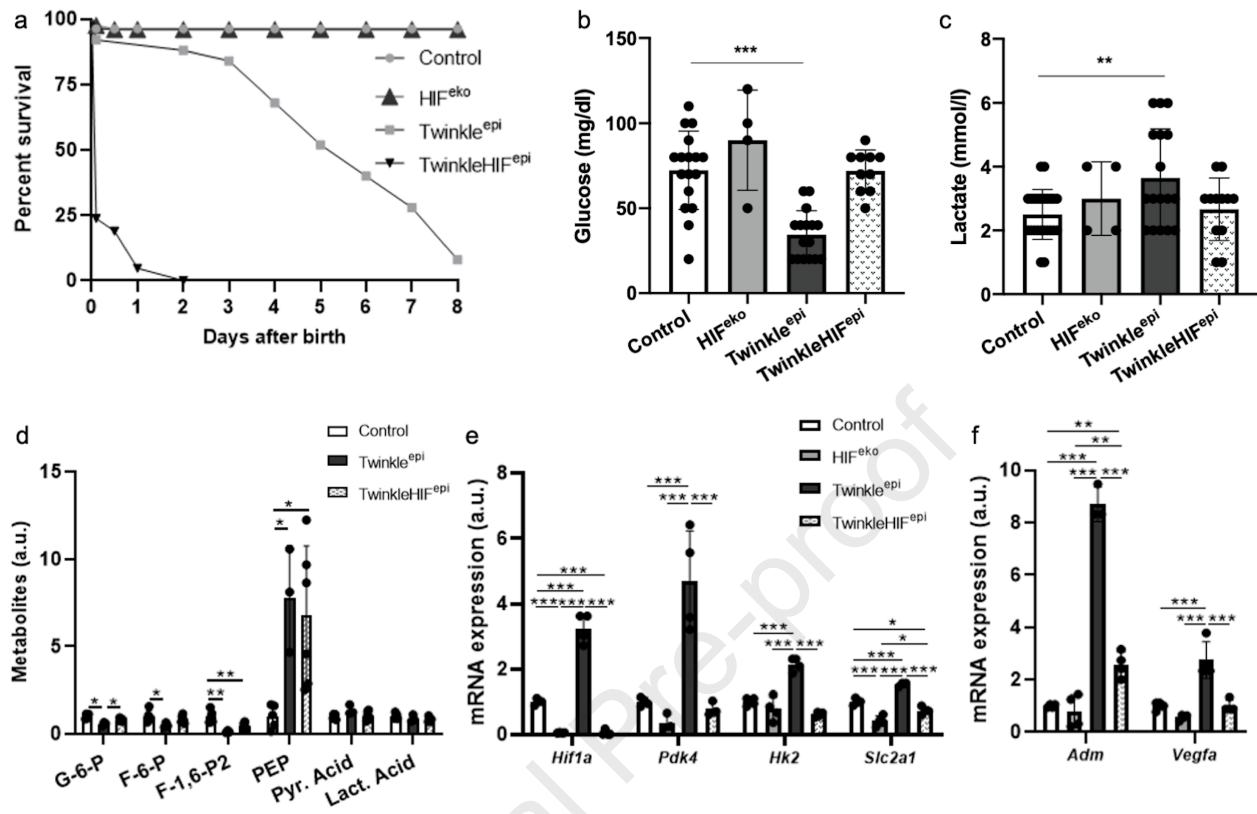


Figure 3

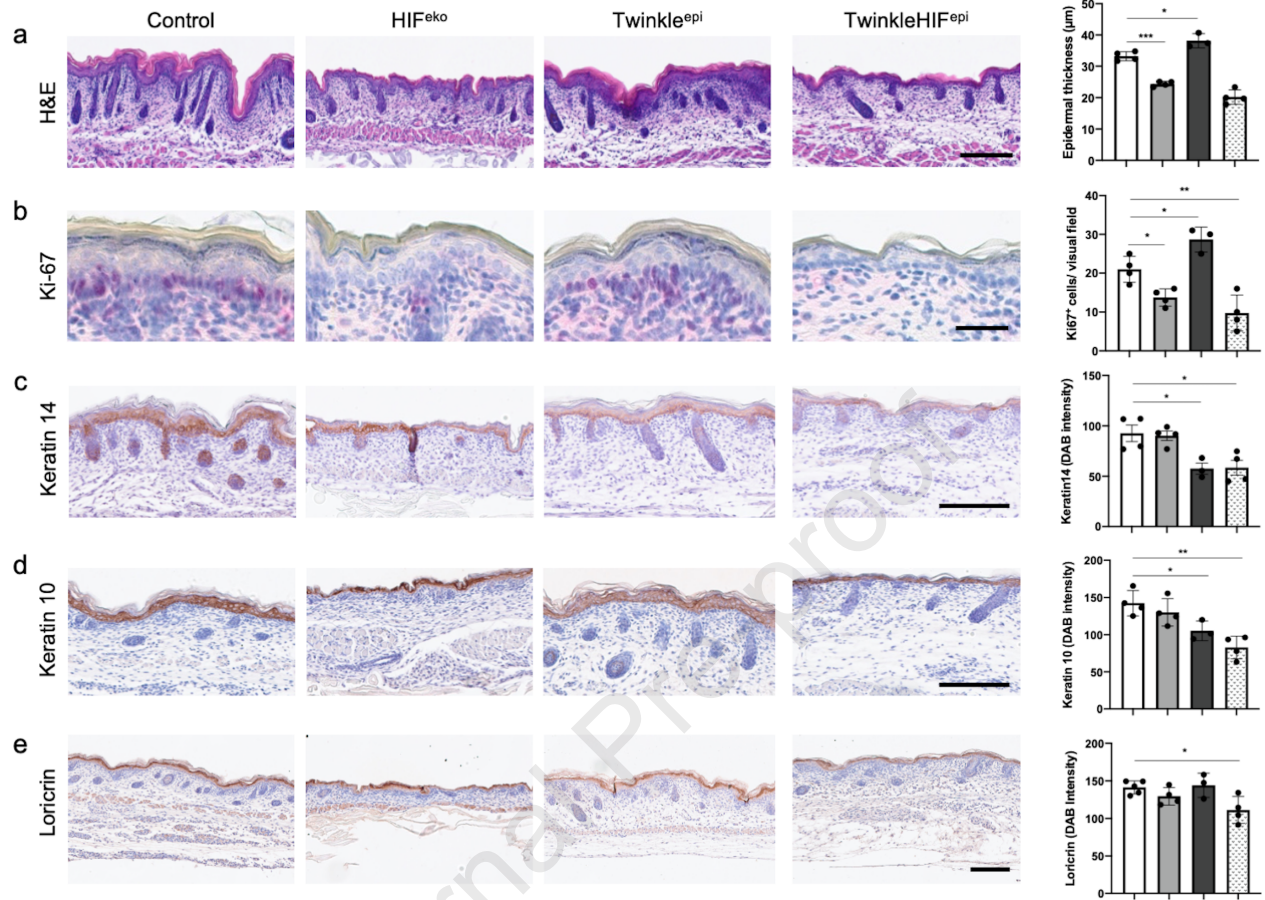


Figure 4

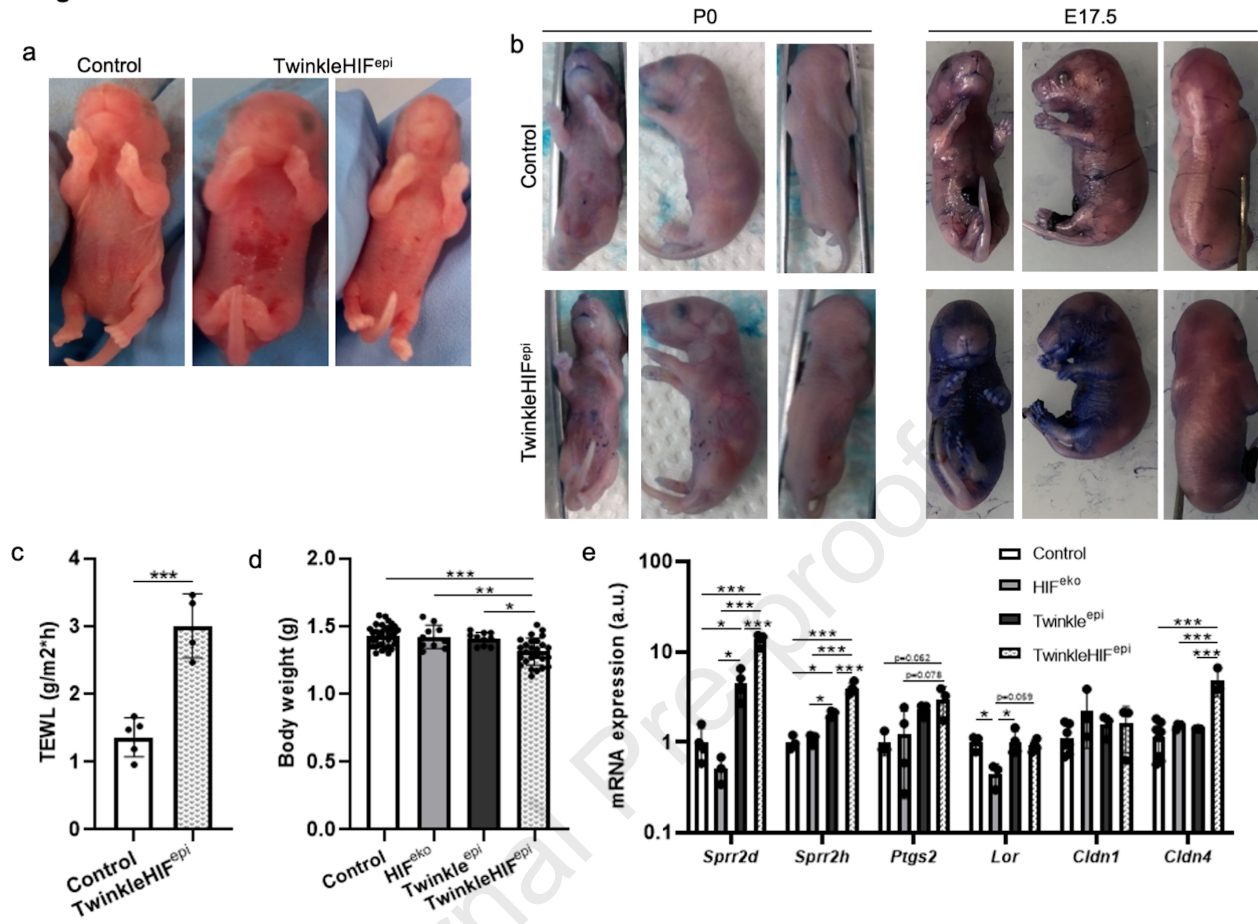


Figure 5

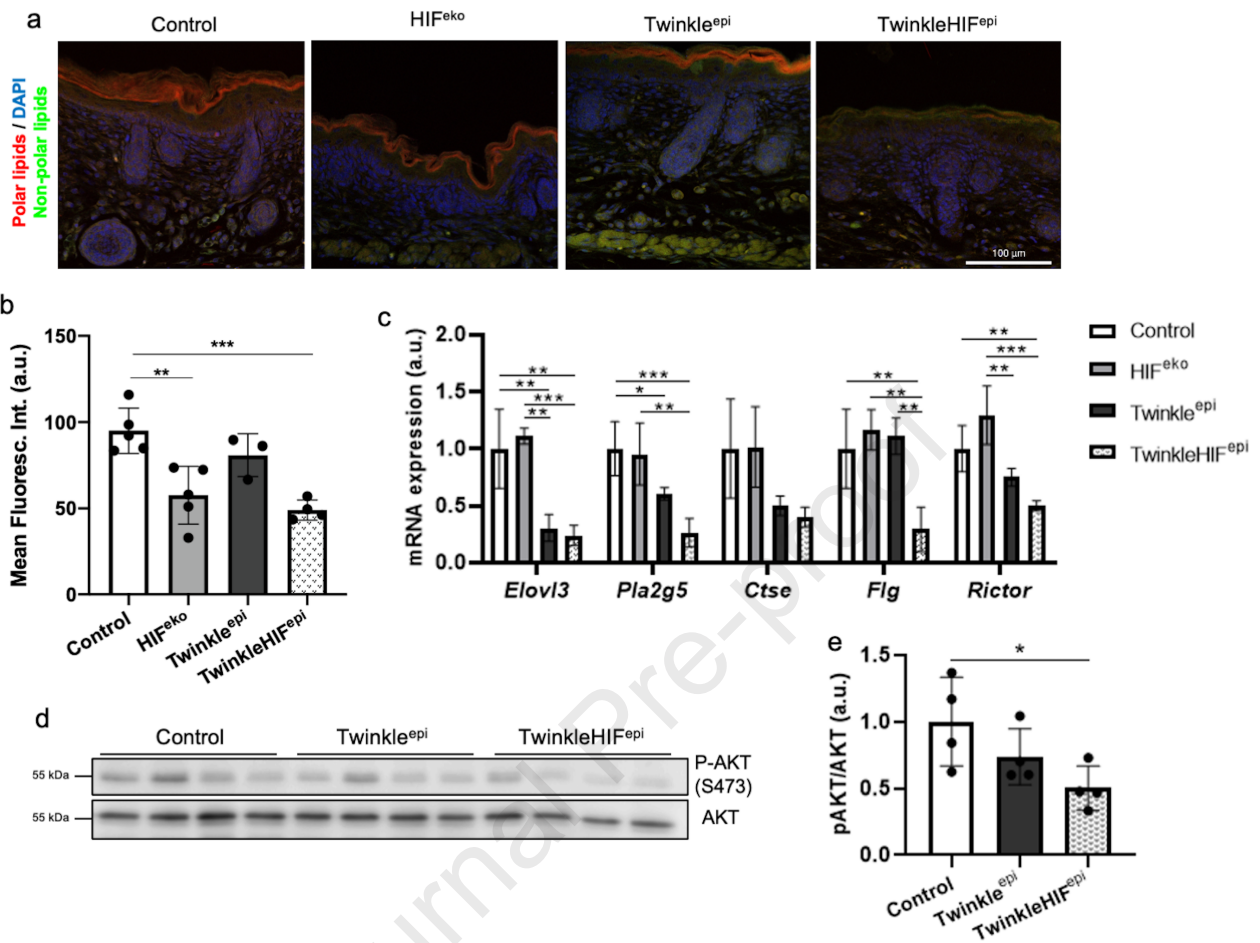
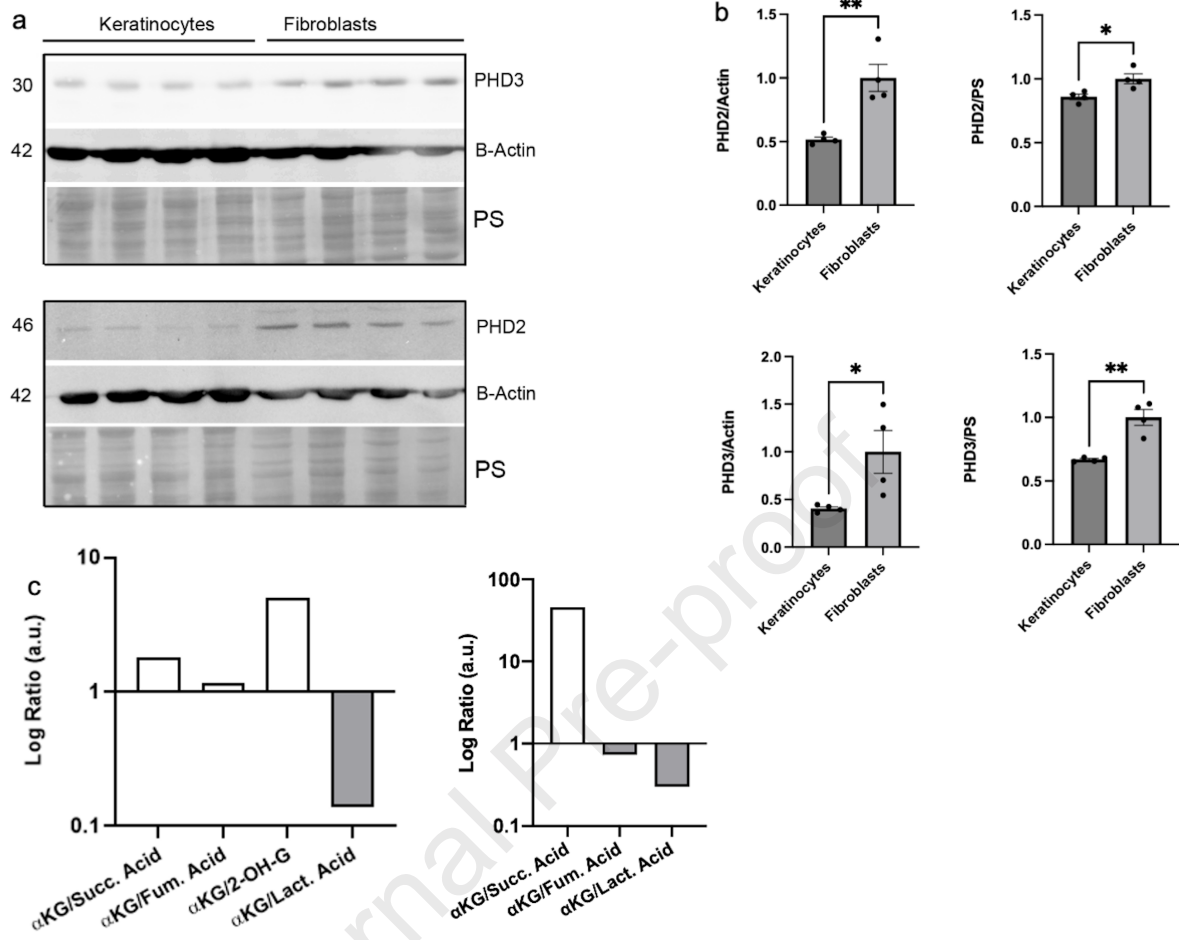
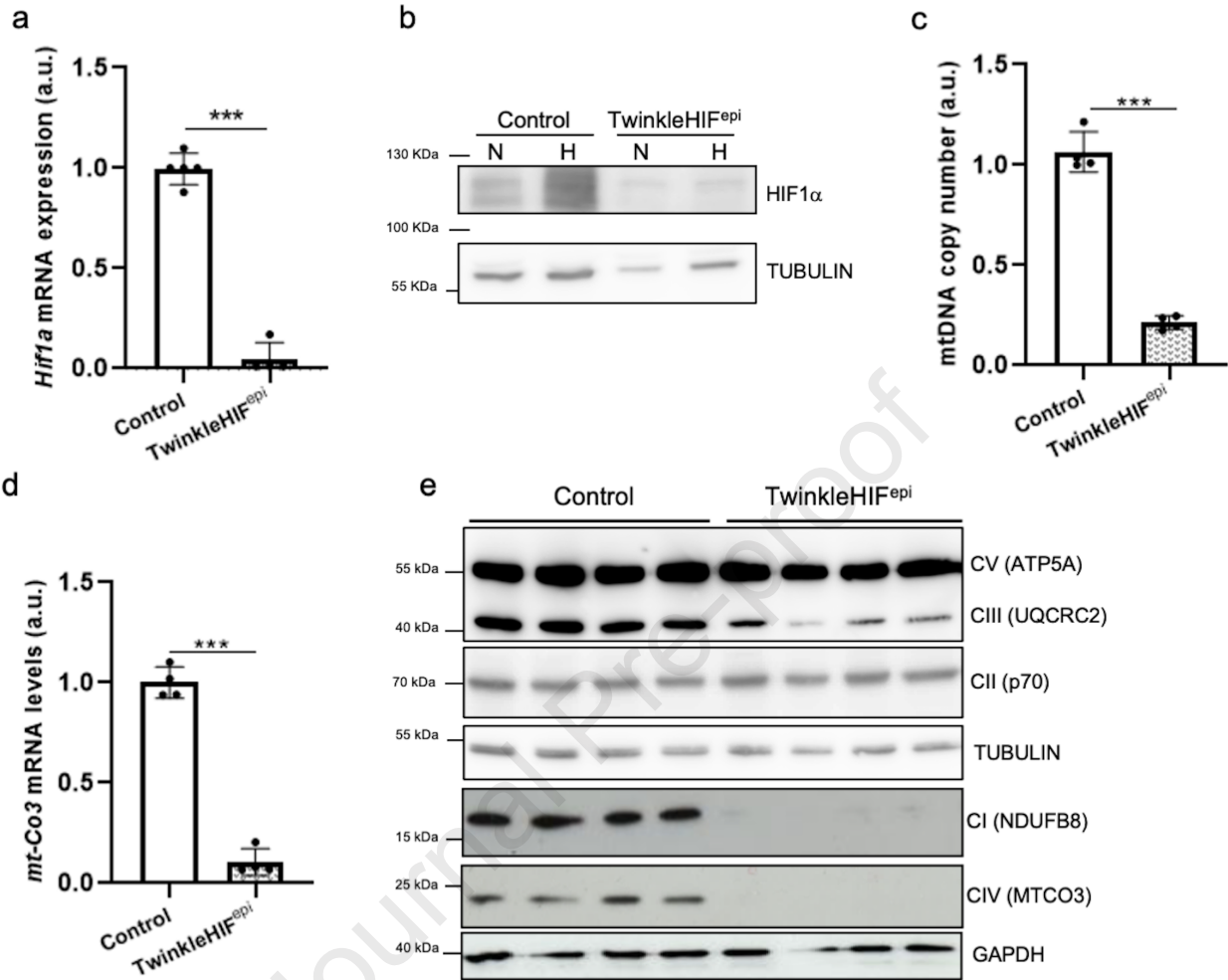


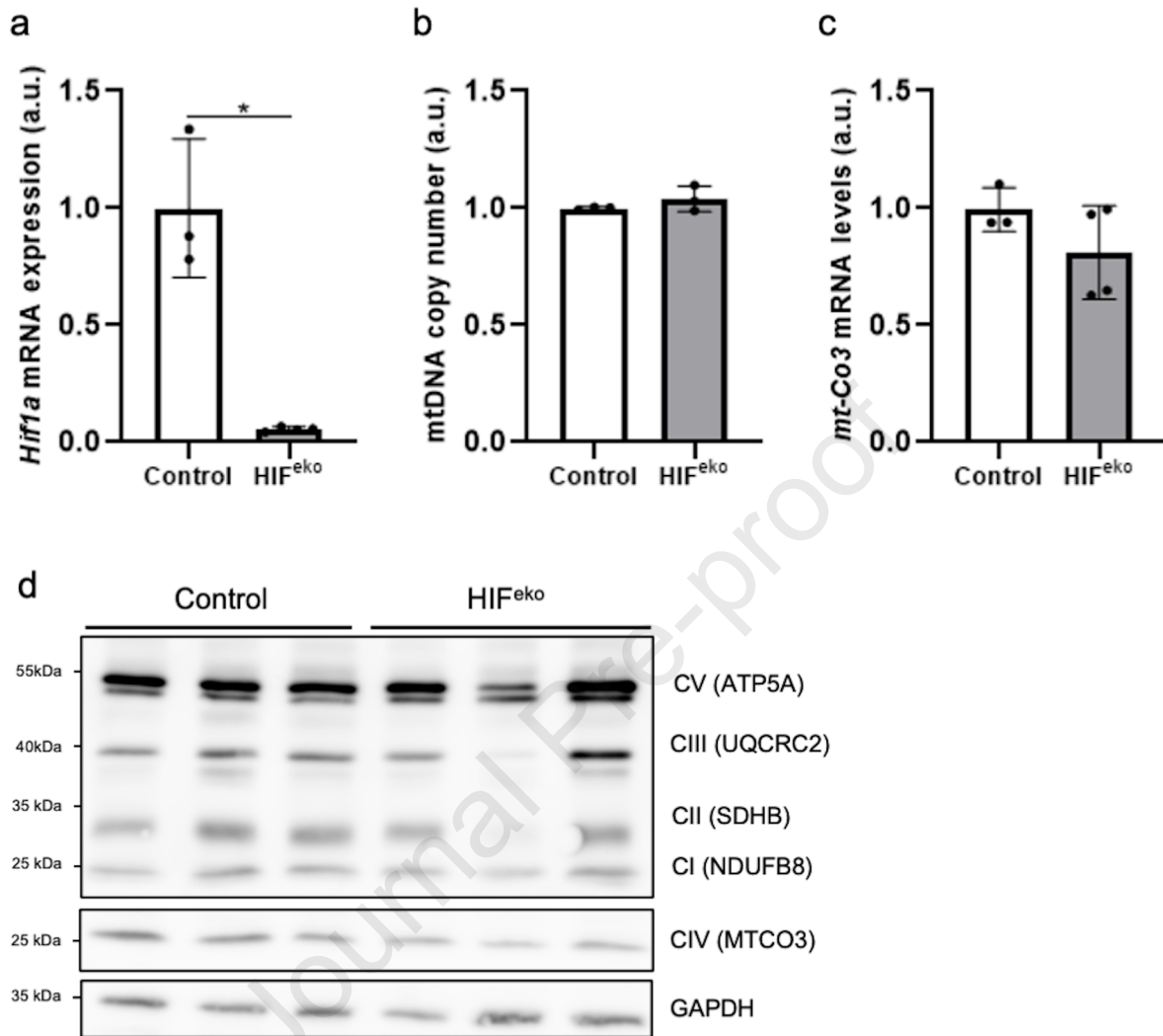
Figure 6



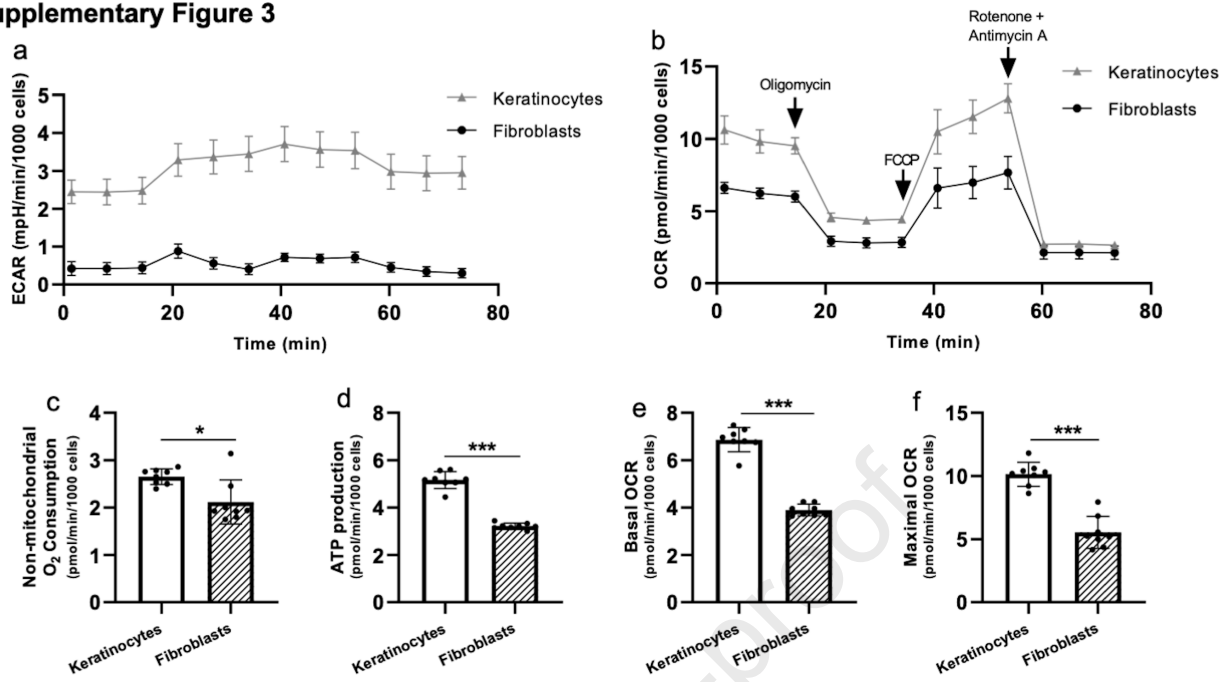
Supplementary Figure 1



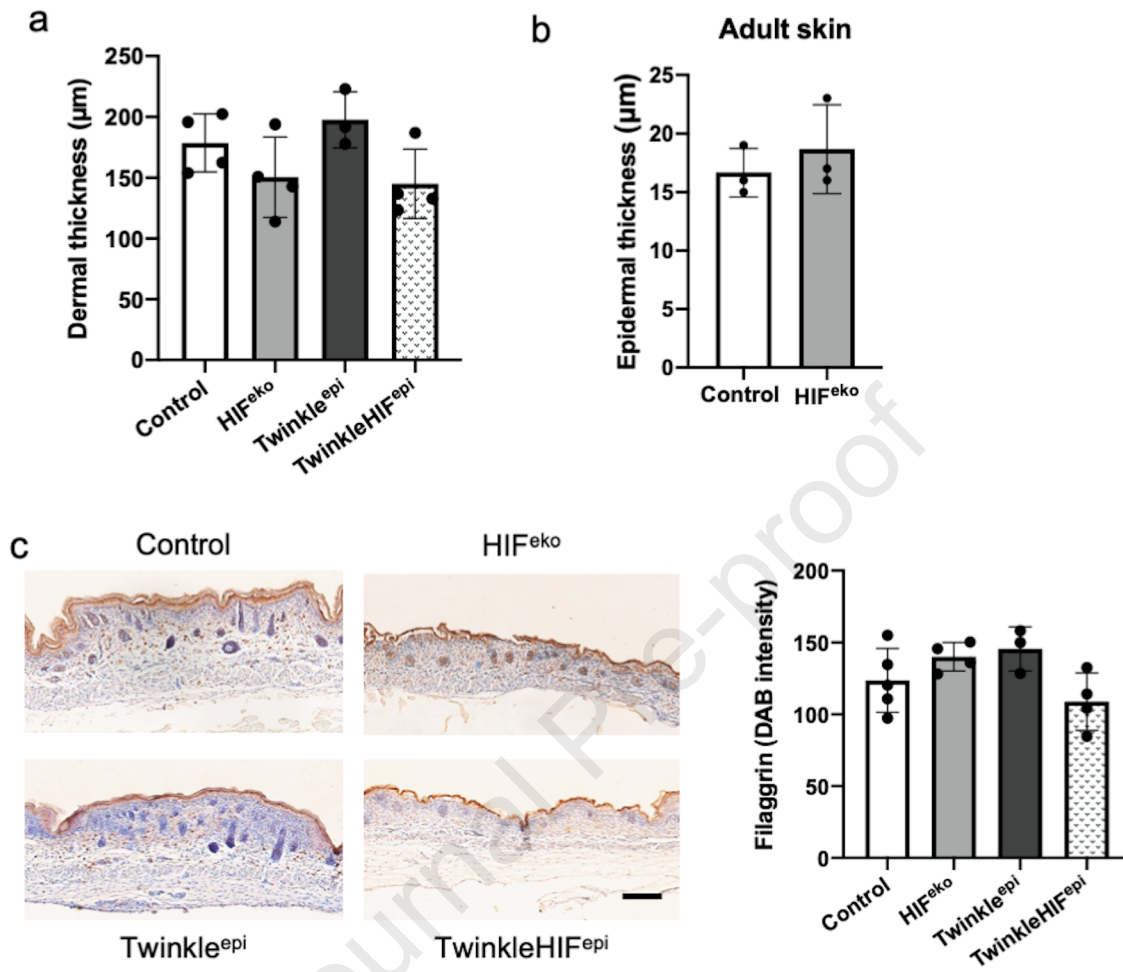
Supplementary Figure 2



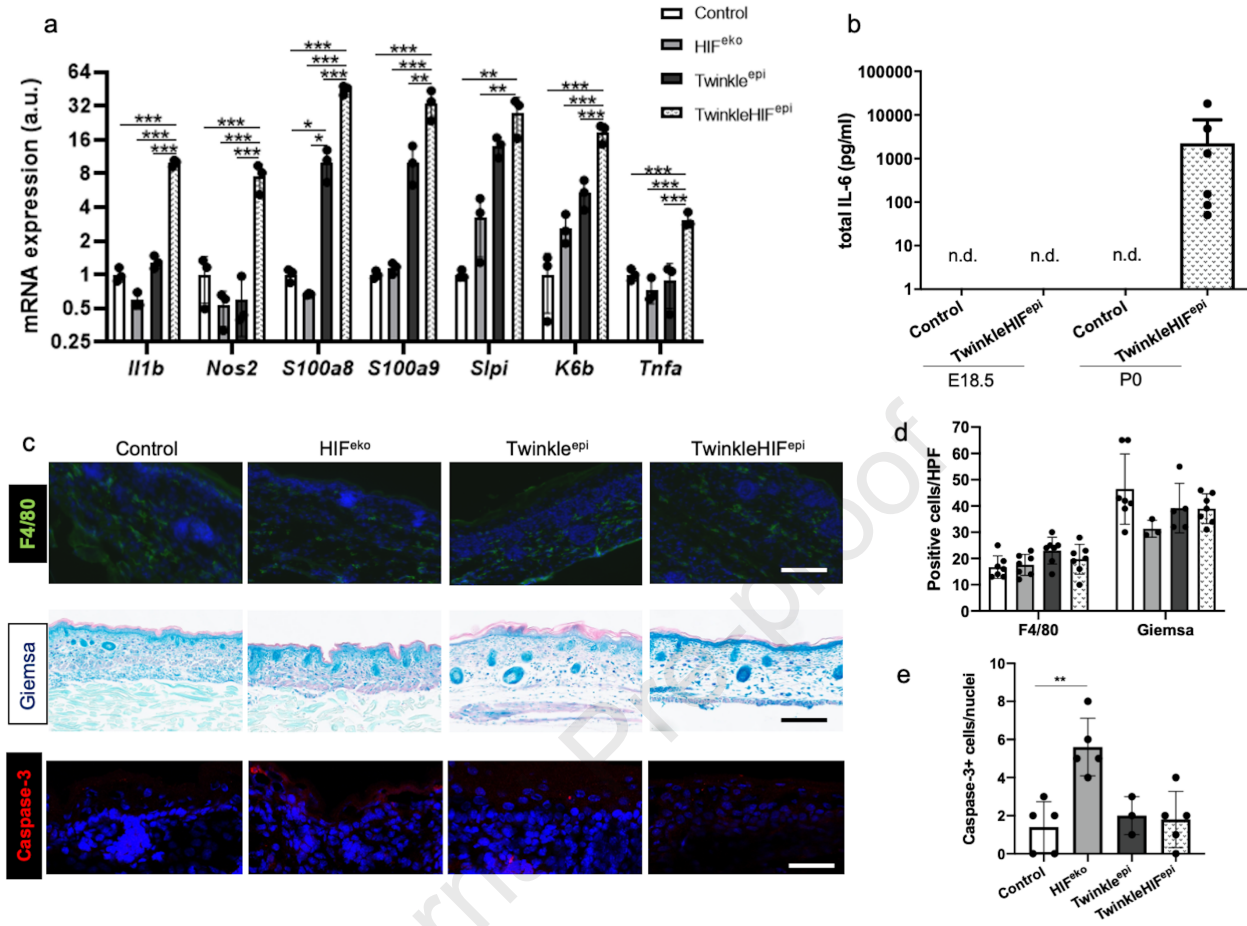
Supplementary Figure 3



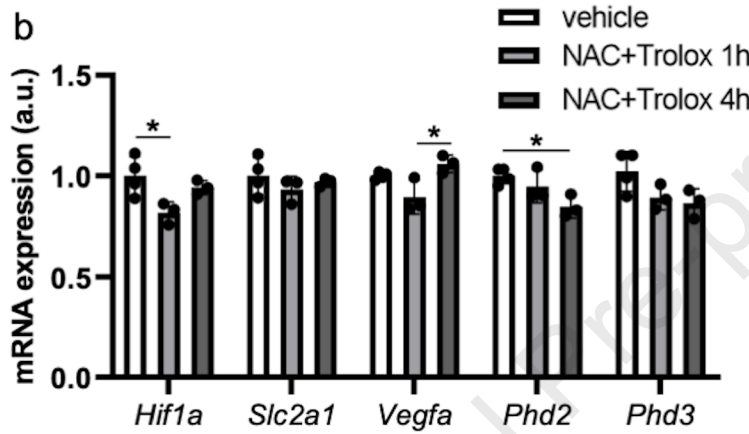
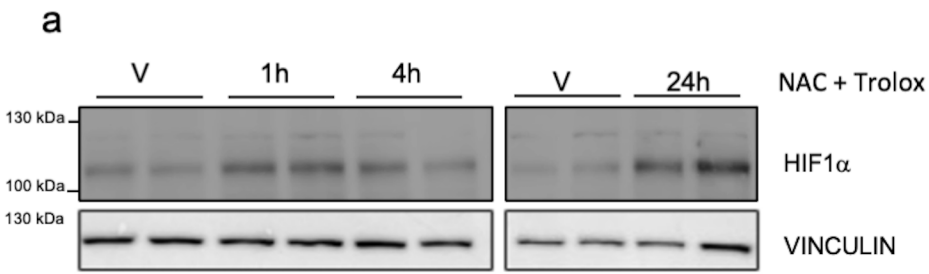
Supplementary Figure 4



Supplementary Figure 5



Supplementary Figure 6



Supplementary Figure Legends

Supplementary Figure 1.

(a) RT-qPCR showing *Hif1a* mRNA levels in control and TwinkleHIF^{epi} newborn epidermis at birth (n=4-5 mice per genotype). (b) Representative immunoblot of HIF-1 α protein in control and TwinkleHIF^{epi} epidermal keratinocytes isolated and cultured in normoxic (N, 21% O₂ 6 h) or hypoxic (H, 1% O₂ 6 h) conditions. Tubulin was used as loading control. (c) qPCR for mtDNA copy number quantification in control and TwinkleHIF^{epi} epidermis at birth (n=3-4 mice per genotype). (d) RT-qPCR showing *mt-Co3* mRNA levels in control and TwinkleHIF^{epi} newborn epidermis at birth (n=4 mice per genotype). (e) Immunoblot of representative subunits (in brackets) of the five OXPHOS complexes (C) in control and TwinkleHIF^{epi} epidermis of newborn mice. Tubulin or GAPDH were used as loading controls according to molecular weight. (a, c, d) Mean \pm standard deviation. Student's t-test; **, p-value < 0.01, ***, p-value < 0.001.

Supplementary Figure 2.

(a) RT-qPCR showing *Hif1a* mRNA levels in control and HIF^{eko} newborn epidermis at birth (n=3-4 mice per genotype). (b) qPCR for mtDNA copy number quantification in control and HIF^{eko} epidermis at birth (n=3 mice per genotype). (c) RT-qPCR showing *mt-Co3* mRNA levels in control and HIF^{eko} newborn epidermis at birth (n=3-4 mice per genotype). (d) Immunoblot of representative subunits (in brackets) of the five OXPHOS complexes (C) in control and HIF^{eko} epidermis of newborn mice. GAPDH was used as loading control. (a-c) Mean \pm standard deviation. Student's t-test; *, p-value < 0.05.

Supplementary Figure 3.

Graphs displaying (a) extracellular acidification rate (ECAR), (b) oxygen consumption rate (OCR) and (c-f) derived bioenergetic parameters of primary keratinocytes and fibroblasts in culture (n=8 biological replicates per cell type). For interpretation, see Supplementary Results section. (c-f) Mean \pm standard deviation. Student's t-test; *, p-value < 0.05, ***, p-value < 0.001.

Supplementary Figure 4.

(a) Dermal thickness of control, HIF^{eko}, Twinkle^{epi} and TwinkleHIF^{epi} newborn skin at birth (n=3-4 mice per genotype). (b) Epidermal thickness of control and HIF^{eko} adult mice (n=3 mice per genotype). (c) Immunostaining and quantification of filaggrin of control (n=5), HIF^{eko} (n=4), Twinkle^{epi} (n=3) and TwinkleHIF^{epi} (n=4) newborn skin at birth. Bar = 100 μ m. (a-c) Mean \pm standard deviation.

Supplementary Figure 5.

(a) RT-qPCR showing mRNA levels for *Ii1b*, *Nos2*, *S100a8*, *S100a9*, *Slpi*, *K6b*, *Tnfa* in control, HIF^{eko}, Twinkle^{epi} and TwinkleHIF^{epi} newborn epidermis (n=3 mice per genotype). (b) Total IL-6 levels measured in control (n=3) and TwinkleHIF^{epi} (n=12) serum at embryonic (E) day 18.5 and birth. Non-detectable levels were indicated as n.d. (c) Immunofluorescence for F4/80 (macrophages), bar = 50 μ m, Giemsa staining (mast cells), bar = 100 μ m, and immunofluorescence of caspase-3 positive cells in control, HIF^{eko}, Twinkle^{epi}, and TwinkleHIF^{epi} newborn skin. Bar = 100 μ m. HPF = high-power field. (d) Quantification of macrophages and mast cells (n=3-7 mice per genotype). (e) Quantification of caspase-3 positive cells (n=3-5 mice per genotype). (a-e) Mean \pm standard deviation. One-way ANOVA, Tukey's post-hoc test; *, p-value < 0.05; **, p-value < 0.01; ***, p-value < 0.001.

Supplementary Figure 6.

(a) Representative immunoblot of HIF-1 α in keratinocytes treated with vehicle (V) or ROS scavengers for the indicated time. Vinculin was used as high molecular weight loading control. (b) RT-qPCR showing *Hif1a*, *Slc2a1*, *Vegfa*, *Phd2* and *Phd3* mRNA levels in *wild-type* keratinocytes treated with vehicle or ROS scavengers for the indicated time. Mean \pm standard deviation. One-way ANOVA, Tukey's post-hoc test; *, p-value < 0.05.

Supplementary Results

The aerobic-glycolytic phenotype of wild-type keratinocytes was confirmed by measuring extracellular acidification rate (ECAR; analogous to lactate production, Figure S3a), where keratinocytes produced 3x more lactate when compared to dermal

fibroblasts. However, keratinocytes also consumed 75% more oxygen (Figure S3b), consequently show a 75% higher rate of ATP production by OXPHOS (Figure S2c-f) in order to support their higher proliferation rate.

Our measurements show that both the basal and the maximally possible respiration rates were higher in keratinocytes (Figure S3e, f), indicating that proliferating keratinocytes have a high energy demand, which they cover in large part by oxidative phosphorylation. Interestingly, non-mitochondrial oxygen consumption is also increased in keratinocytes compared to fibroblasts (Figure S3c).

Supplementary Material and Methods

Animal generation and experiments

All animal experiments were approved by the animal care committee of the University of Cologne and local government authorities (Bezirksregierung Köln; Landesamt für Natur, Umwelt und Verbraucherschutz [LANUV], Recklinghausen; Az.81-02.04.2019.A101; 84-02.04.2015.A405). Keratin 14-Cre mice (Hafner et al., 2004), R26-K320E-Twinkle^{loxP/loxP} (Baris et al., 2015) and Hif1 α ^{loxP/loxP} mice (Boutin et al., 2008) were previously described. K320E-Twinkle^{epi} mice, called Twinkle^{epi} mice here (K14-Cre^{+/-}; K320E-Twinkle^{loxP/wt}), were generated as previously described (Weiland et al., 2018). K320E-Twinkle-Hif1 α ^{epi} mice (K14-Cre^{+/-}; K320E-Twinkle^{loxP/wt}; Hif1 α ^{loxP/loxP}) and Hif1 α ^{epi} mice (K14-Cre^{+/-}; Hif1 α ^{loxP/loxP}) were generated by crossing these mouse lines. Littermates with the same genotype, but lacking Cre recombinase were used as controls. Genotyping was performed on tail or ear biopsies using primers available upon request. When indicated, embryos were obtained by caesarean section.

Measurements of blood glucose and lactate levels

Blood glucose and lactate levels were measured in serum, freshly prepared from blood of newborn mice using the Cobas C 702 system (Roche Diagnostics, Indianapolis, Indiana, United States) and the Radiometer ABL 800 Flex blood gas analyzer (Radiometer America, Brea, California 92821, USA).

Tissue collection, histological and immunohistochemical analyses

Back and ventral skin samples from mice were embedded at the indicated time points in optimal cutting temperature compound (Tissue-Tek; Sakura, Alphen aan den Rijn, The Netherlands) or fixed in 4% paraformaldehyde and embedded in paraffin. Hematoxylin-eosin staining was performed on 5- μ m slides to assess skin morphology. Epidermal and dermal thickness was measured using Image J software (ImageJ software, version 1.52, National Institutes of Health, Bethesda, MD, USA). At least five randomized areas of each section were chosen (Leica SCN400 Slidescanner and Leica SlidePath Gateway Client LAN 2b4 Software, Leica Microsystems, Wetzlar, Germany), and five to ten measurements were performed in each area. Giemsa staining and quantification (ImageJ software, version 1.52, National Institutes of Health, Bethesda, MD) were used for mast cell numbers. For immunostaining, endogenous peroxidase activity was blocked in paraffin sections with methanol:H₂O₂ (29:1), followed by overnight incubation at 4°C in 5% fetal bovine serum and primary antibodies against keratin 14 (1:2000, 905301, Biolegend, Waltham, USA), keratin 10 (1:2000, 905401, Biolegend, Waltham, USA), loricrin (1:2000, 905101, Biolegend, Waltham, USA), filaggrin (1:1000, B257576, Biolegend, Waltham, USA) and Ki67 (1:100, M7249, Dako, Vector Laboratories, Inc., Burlingame, CA). Slides were washed with PBS and then incubated with biotin-conjugated secondary antibodies for 1 h. The reaction was visualized with the avidin-biotin complex (ABC) kit (Dako, Vectastain Elite; Vector Laboratories, Inc., Burlingame, CA) using diaminobenzidine for peroxidase reaction. Slides were counterstained with hematoxylin and mounted. Positive Ki67 nucleus quantification was performed counting the positive nuclei per visual field in the basal epidermal layer in five to eight random areas per section. For quantification of K14, K10, loricrin and filaggrin expression in the epidermis the corresponding layers were manually marked, respectively. After inverting to grey-white scales the mean staining intensity was measured by Image J. Epidermal sheets were prepared by incubating skin in 1 mg/ml dispase II (Roche, Basel, Switzerland) for 1 h at room temperature, separating them from the dermis, then snap-freezing for follow-up analyses.

Immunofluorescence

Immunofluorescence experiments were performed as previously described (Boix et al., 2016) using F4/80 (1:100, MCA497, BioRad, Hercules, CA) as primary antibody

for the detection of macrophages and Caspase-3 (1:200, 9664S, Cell Signaling, Danvers, USA) for detection of apoptotic cells. Nile-red staining (0.1%, Sigma, St. Louis, USA) was performed for 5 min together with DAPI at room temperature. Pictures were taken at 40x magnification with the Leica TCS SP8 microscope (Leica Microsystems, Wetzlar, Germany). For the polar lipids, mean fluorescence intensity was measured from the pre-selected stratum corneum area (ImageJ software, version 1.52, National Institutes of Health, Bethesda, MD).

Quantification of mtDNA copy number

Total DNA was extracted with the DNeasy Blood & Tissue Kit (Qiagen, Hilden, Germany). The mtDNA copy number was measured by qPCR as previously described (Neuhaus et al., 2017).

Isolation and culture of primary keratinocytes and fibroblasts

Keratinocytes and fibroblasts were isolated from newborn mouse skin following epidermal-dermal separation by overnight incubation in 5 mg/ml dispase II (Roche, Basel, Switzerland) at 4°C as previously described (Rubsam et al., 2017), and dermal digestion by collagenase at 37°C. Standard conditions for primary cells were set at 32°C (keratinocytes) and 37°C (fibroblasts) and 5% CO₂ in DMEM/HAM's F12 (FAD) medium with low Ca²⁺ (50 µM) (Merck Millipore, Burlington, USA) supplemented with 10% FCS (chelated), penicillin (100 U ml⁻¹), streptomycin (100 µg ml⁻¹, Biochrom A2212, Merck Millipore, Burlington, USA), adenine (1.8 × 10⁻⁴ M, SIGMA A3159, St. Louis, USA), L-glutamine (2 mM, Biochrom K0282, Merck Millipore), hydrocortisone (0.5 µg ml⁻¹, Sigma H4001), EGF (10 ng ml⁻¹, Sigma E9644), cholera enterotoxin (10⁻¹⁰ M, Sigma C-8052), insulin (5 µg ml⁻¹, Sigma I1882), and ascorbic acid (0.05 mg ml⁻¹, Sigma A4034). For normoxic and hypoxic (1% pO₂) conditions, keratinocytes were incubated for 6 h at 37°C. Wildtype keratinocytes were plated onto normal and gas permeable Petriperm® cell culture dishes, both in increasing density of 1, 2, and 4 million cells/well. ROS scavenger treatment was performed on cultured wild-type keratinocytes for 1, 4 and 24 h with 2.5 mM each N-acetyl cysteine and 200 µM trolox.

RNA isolation and quantitative RT-PCR

Epidermal and dermal sheets from newborn mice were homogenized using a mixer mill (Retsch, Germany; 5 minutes, 30 Hz). Total RNA was then isolated using Trizol

(Thermo Fisher, Waltham, USA). cDNA was synthesized using the RevertAid First Strand cDNA Synthesis Kit (Thermo Fisher). Quantitative RT-PCR was performed using specific oligonucleotides (available upon request) and Power SYBR Green PCR Master Mix (Applied Biosystem, Waltham, USA) in an Applied Biosystems StepOnePlus Real Time PCR system. At least three biological replicates were used for each experimental group, and technical triplicates were assessed to calculate the mean value \pm standard deviation.

Immunoblotting

Whole-protein lysates from epidermal and dermal sheets were prepared and separated by SDS-PAGE as described (Baris et al., 2011). Whole-cell extracts of keratinocytes and fibroblasts were prepared as described (Fuhrmann et al., 2015) (Müller-Edenborn et al., 2015). Primary antibodies were derived against HIF-1 α (1:500, GTX127309, GeneTex or 1:500, 36169, Cell Signaling, Danvers, USA), PHD2 (1:1000, 19886-1-AP, Proteintech), PHD3 (1:1000, NB-100-139, Novus), total AKT (1:1000, 9272, Cell Signaling, Danvers, USA), phospho AKT (1:500, 9271, Cell Signaling, Danvers, USA), total OXPPOS Rodent WB Antibody Cocktail (1:4000, ab110413, Abcam, Cambridge, GB), p70 (1:2000, 459200, Invitrogen), mtCO3 (1:2000, ab110259), Tubulin (1:2000, T4026, Sigma Aldrich), β -Actin (1:5000, A1978, Sigma Aldrich), Vinculin (1:5000, 66305-1-Ig, ProteinTech, Pearl St, USA) and GAPDH (1:5000, AB2302, Merk Millipore). Signals were detected using the Western Lightning Plus-ECL, Enhanced Chemiluminescence Substrate (Perkin Elmer, Waltham, MA), and ImageQant LAS500 chemiluminescence CCD Camera (GE Healthcare Bio-Sciences, Pittsburgh, PA).

Cytokine profiling

Blood samples were centrifuged at 1500 g and 4°C for 10 minutes, the serum was collected and stored at -20°C until usage. Cytometric Bead Array Detection System using Mouse/Rat Soluble Protein Master Buffer Kit (cat. no. 558266) was applied to measure IL-6 (Mouse Flex Set cat. no. 558301) levels in serum samples according to the manufacturer's protocol. Measurements were performed using the FACSCanto™ II flow cytometer and data was analyzed using the FCAP Array v3 software (Becton Dickinson) (Probst et al., 2018).

Epidermal barrier function assays

Epidermal dye permeability assays were performed with 1% toluidine blue dye (Sigma Aldrich) at the indicated ages as described (Byrne et al., 2010). Transepidermal water loss (TEWL) was measured in newborn ventral skin using a Tewameter (Courage) and performed according to the manufacturer's instructions.

Energy metabolism

To characterize their energy metabolism, oxygen consumption (OCR) and extracellular acidification rate (ECAR) was measured in keratinocytes and fibroblasts (so-called mito stress test; Seahorse XF96 Bioanalyzer, Town, State). Cells were seeded at a density of 15,000 cells per well (n=8). Prior to the assay the cells were washed carefully with Seahorse assay media supplemented with glucose, sodium pyruvate and L-glutamine. The cells were then allowed to adapt to the assay medium (XF Base Media Minimal DMEM, pH 7.4, supplemented with 10 mM glucose, 1 mM pyruvate and 2 mM glutamine) for one hour. To characterize respiratory chain function, oligomycin was injected (1 μ M), followed by FCCP (2 μ M FCCP) and rotenone/antimycin A (0.5 μ M each). Then, Hoechst dye was added, and cells were counted 25 min later using an automated cell imaging software (Agilent, Town, State). OCR and ECAR data were normalized to the number of living cells per well; 8 technical replicates were averaged to get the final graphs.

Anion-exchange chromatography mass Spectrometry (AEX-MS)

Freshly isolated keratinocytes were seeded in collagen-coated plates one day before metabolite isolation. Cells were washed twice with PBS and incubated with pre-cooled extraction buffer (methanol:acetonitrile:water, 40:40:20) at -20°C for 10 minutes. Samples were collected using a cell scraper and the extraction was repeated using the same extraction buffer. Fresh frozen epidermal tissue was homogenized using a ball mill (Retsch MM400) after precooling the samples in the holder with liquid nitrogen. Extraction buffer was the same as described above. Proteins were spun down by centrifugating samples at 21,000 g for 10 min and the supernatant was used as follows. Extracted metabolites were re-suspended in 150 μ l of UPLC/MS grade water (Biosolve), of which 100 μ l were transferred to polypropylene autosampler vials

(Chromatography Accessories Trott, Kriftel, Germany) before AEX-MS analysis. The samples were analysed using a Dionex ion chromatography system (Integrion Thermo Fisher Scientific) as described previously (Schwaiger et al., 2017). In brief, 5 μ l of polar metabolite extract were injected in push partial mode, using an overfill factor of 1, onto a Dionex IonPac AS11- HC column (2 mm \times 250 mm, 4 μ m particle size, Thermo Fisher Scientific) equipped with a Dionex IonPac AG11-HC guard column (2 mm \times 50 mm, 4 μ m, Thermo Fisher Scientific). The column temperature was held at 30°C, while the auto sampler was set to 6°C. A potassium hydroxide gradient was generated using a potassium hydroxide cartridge (Eluent Generator, Thermo Scientific, Waltham, USA), which was supplied with deionized water (Millipore). The metabolite separation was carried at a flow rate of 380 μ l/min, applying the following gradient conditions: 0-3 min, 10 mM KOH; 3-12 min, 10-50 mM KOH; 12-19 min, 50-100 mM KOH; 19-22 min, 100 mM KOH, 22-23 min, 100-10 mM KOH. The column was re-equilibrated at 10 mM for 3 min. For the analysis of metabolic pool sizes the eluting compounds were detected in negative ion mode using full scan measurements in the mass range m/z 77 – 770 on a Q-Exactive HF high resolution MS (Thermo Fisher Scientific). The heated electrospray ionization (HESI) source settings of the mass spectrometer were: Spray voltage 3.2 kV, capillary temperature was set to 300°C, sheath gas flow 50 AU, aux gas flow 20 AU at a temperature of 330°C and a sweep gas flow of 2 AU. The S-lens was set to a value of 60. The semi-targeted LC-MS data analysis was performed using the TraceFinder software (Version 4.1, Thermo Fisher Scientific). The identity of each compound was validated by authentic reference compounds, which were measured at the beginning and the end of the sequence. For data analysis the area of the deprotonated $[M-H]^{-1}$ or doubly deprotonated $[M-2H]^{-2}$ monoisotopologue mass peaks of every required compound were extracted and integrated using a mass accuracy <5 ppm and a retention time tolerance of <0.05 min as compared to the independently measured reference compounds. These areas were then normalized to the internal standards, which were added to the extraction buffer, followed by a normalization to the fresh weight of the analyzed sample. Five replicates were used. The ratios between α -ketoglutarate and succinate, fumarate, 2-OH-glutarate or lactate were calculated with the mean of all replicates.

Statistics

Experimental data were analyzed using GraphPad Prism 8.0 (GraphPad Software Ink, San Diego, USA). Unless otherwise mentioned, mean values \pm standard deviation are shown. For comparisons between two experimental groups, we used Student's unpaired two-tailed t-test. For comparisons among more than two experimental groups, one-way analysis of variance (ANOVA) was used, which, if statistically significant, was followed by a post hoc Tukey's multiple comparison test. p-values less than 0.05 were considered statistically significant. * p-value<0.05; ** p-value<0.01; ***p-value<0.001. When normality of distribution could not be assessed because of limited size of some sample groups (n=3-8), statistical analysis was performed with the assumption of normally distributed data.

Supplementary References

Baris OR, Ederer S, Neuhaus JF, von Kleist-Retzow JC, Wunderlich CM, Pal M, et al. Mosaic Deficiency in Mitochondrial Oxidative Metabolism Promotes Cardiac Arrhythmia during Aging. *Cell Metab* 2015;21(5):667-77.

Baris OR, Klose A, Kloepper JE, Weiland D, Neuhaus JF, Schauen M, et al. The mitochondrial electron transport chain is dispensable for proliferation and differentiation of epidermal progenitor cells. *Stem Cells* 2011;29(9):1459-68.

Boix J, Sevilla L, Sáez Z, Carceller E, Pérez P. Epidermal Mineralocorticoid Receptor Plays Beneficial and Adverse Effects in Skin and Mediates Glucocorticoid Responses. *J Invest Dermatol* 2016;Dec;136(12):2417-2426.

Boutin AT, Weidemann A, Fu Z, Mesropian L, Gradin K, Jamora C, et al. Epidermal sensing of oxygen is essential for systemic hypoxic response. *Cell* 2008;133(2):223-34.

Byrne C, Avillion AA, O'Shaughnessy RF, Welti JC, Hardman MJ. Whole-mount assays for gene induction and barrier formation in the developing epidermis. *Methods Mol Biol* 2010;585:271-86.

Fuhrmann DC, Tausendschon M, Wittig I, Steger M, Ding MG, Schmid T, et al. Inactivation of tristetraprolin in chronic hypoxia provokes the expression of cathepsin B. *Mol Cell Biol* 2015;35(3):619-30.

Hafner M, Wenk J, Nenci A, Pasparakis M, Scharffetter-Kochanek K, Smyth N, et al. Keratin 14 Cre transgenic mice authenticate keratin 14 as an oocyte-expressed protein. *Genesis* 2004;38(4):176-81.

Müller-Edenborn K, Léger K, Glaus Garzon JF, Oertli C, Mirsaidi A, Richards PJ, et al. Hypoxia attenuates the proinflammatory response in colon cancer cells by regulating I κ B. *Oncotarget* 2015;Aug 21;6(24):20288-301.

Neuhaus JF, Baris OR, Kittelmann A, Becker K, Rothschild MA, Wiesner RJ. Catecholamine Metabolism Induces Mitochondrial DNA Deletions and Leads to Severe Adrenal Degeneration during Aging. *Neuroendocrinology* 2017;104(1):72-84.

Probst K, Stermann J, von Bomhard I, Etich J, Pitzler L, Niehoff A, et al. Depletion of Collagen IX Alpha1 Impairs Myeloid Cell Function. *Stem Cells*. 2018 Nov;36(11):1752-1763.

Rubsam M, Mertz AF, Kubo A, Marg S, Jungst C, Goranci-Buzhala G, et al. E-cadherin integrates mechanotransduction and EGFR signaling to control junctional tissue polarization and tight junction positioning. *Nat Commun* 2017;8(1):1250.

Schwaiger M, Rampler E, Hermann G, Miklos W, Berger W, Koellensperger G. Anion-Exchange Chromatography Coupled to High-Resolution Mass Spectrometry: A Powerful Tool for Merging Targeted and Non-targeted Metabolomics. *Anal Chem* 2017;89(14):7667-74.

Weiland D, Brachvogel B, Hornig-Do HT, Neuhaus JFG, Holzer T, Tobin DJ, et al. Imbalance of Mitochondrial Respiratory Chain Complexes in the Epidermis Induces Severe Skin Inflammation. *J Invest Dermatol* 2018;138(1):132-40.